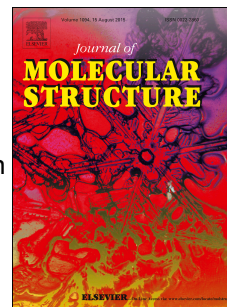


Accepted Manuscript

A critical study of crystal structure, N—H—Br interaction, effect of charge transfer on third-order nonlinear optical properties and optical limiting behaviour of a new crystal: (4-Methoxyphenyl) methanaminium bromide

P. Umarani, A. Thiruvalluvar, C. Ramachandra Raja



PII: S0022-2860(18)30862-7

DOI: [10.1016/j.molstruc.2018.07.043](https://doi.org/10.1016/j.molstruc.2018.07.043)

Reference: MOLSTR 25448

To appear in: *Journal of Molecular Structure*

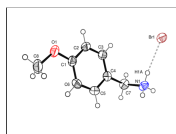
Received Date: 13 April 2018

Revised Date: 11 July 2018

Accepted Date: 12 July 2018

Please cite this article as: P. Umarani, A. Thiruvalluvar, C.R. Raja, A critical study of crystal structure, N—H—Br interaction, effect of charge transfer on third-order nonlinear optical properties and optical limiting behaviour of a new crystal: (4-Methoxyphenyl) methanaminium bromide, *Journal of Molecular Structure* (2018), doi: 10.1016/j.molstruc.2018.07.043.

This is a PDF file of an unedited manuscript that has been accepted for publication. As a service to our customers we are providing this early version of the manuscript. The manuscript will undergo copyediting, typesetting, and review of the resulting proof before it is published in its final form. Please note that during the production process errors may be discovered which could affect the content, and all legal disclaimers that apply to the journal pertain.



ACCEPTED MANUSCRIPT

A critical study of crystal structure, N—H---Br interaction, effect of charge transfer on third-order nonlinear optical properties and optical limiting behaviour of a new crystal : (4-Methoxyphenyl) methanaminium bromide

P. Umarani^a, A. Thiruvalluvar^b and C. Ramachandra Raja^{a,*}

^aGovernment Arts College (Autonomous), Kumbakonam 612 002, Tamilnadu, India

^bKunthavai Naacchiyaar Government Arts College for Women (Autonomous), Thanjavur 613 007, Tamilnadu, India.

* Correspondence E-mail: crrajaphy@gmail.com

Abstract

A new crystal, (4-Methoxyphenyl) methanaminium bromide (4MPMAB) was successfully developed by suitably functionalising the counter anion for nonlinear optical applications. Structural analysis was carried out and explores the monoclinic crystal system of $P2_1/c$ space group. The methoxy group of the cation is co-planar with the phenylene moiety with an r.m.s deviation of 0.0294 Å from the mean plane (C1—C8/O1). The donor mesomeric effect of methoxy group is revealed. The strong bonding nature and intermolecular N—H---Br interaction between the ammonium cation and the halide anion are evidenced. In addition to that, C—H---Br and C—H--- π interactions are also observed. As the protonation takes place by the hydrogen of hydrobromic acid (HBr), the contribution of HBr is highlighted in the formation of the 4MPMAB crystal. Powder X-ray diffraction (PXRD) study authenticates the good crystalline nature of the sample. Fourier transform infrared (FT-IR), ¹H and ¹³C Nuclear magnetic resonance (NMR) spectral study ascertained the functional groups, the formation of the molecule and the N—H---Br interaction of the grown crystal.

The crystal is stable up to 219 °C. 4MPMAB has soft nature. The crystals have 65 % optical transmission from 330 nm to 1100 nm with estimated optical band gap value of 3.5 eV.

Z-scan study exhibits the higher third-order nonlinearity of 4MPMAB crystal. The influence of charge transfer on third-order nonlinear optical properties were revealed. Further, the optical limiting performance of 4MPMAB crystal has also been investigated.

Keywords

(4-Methoxyphenyl) methanaminium bromide; N—H---Br interaction; NMR; third-order nonlinear optical study; optical limiting behaviour

1. Introduction

In recent years, there has been considerable progress in synthesising nonlinear optical crystals for frequency conversion, optoelectronic modulators, optical disk data storage, optical parametric oscillations and terahertz (THz) wave generation [1-3]. NLO crystals should possess greater nonlinear coefficients, considerable phase matching birefringence, wide optical transmittance, improved optical damage threshold and excellent thermal and mechanical stability [4,5]. Material scientists are keen on tailoring the new NLO crystals based on chemical structure and chemical incorporation, concentrating in the enhancement of above mentioned properties. The third-order (NLO) crystals are least concentrated by the researchers when compared to the extensive research carried out on new structures for second order NLO crystals. At present, the scope for designing and analysing properties for third-order NLO crystals has been intensified. A reasonable good susceptibility is one of the most significant criterion for third-harmonic generation. The improvement in nonlinearity in some crystals are due to the existence of donor-acceptor moieties and the presence of hydrogen bonding between the ions. The presence of hydrogen bonds influence the thermal and mechanical stability of the crystal. [6-12]. In this regard, a halogen-based complex of the 4-

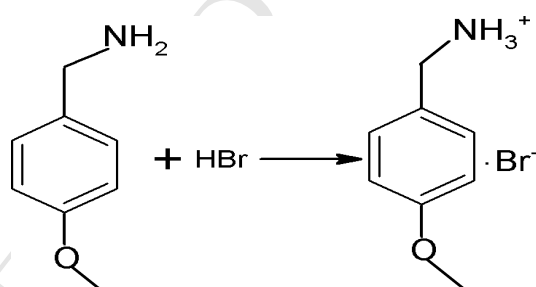
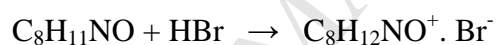
methoxybenzylamine (4MBA) family has been the study of interest. The incorporation of halogen ions into organic framework opens up a new class of materials. As these organic based halogen materials are expected to offer enhanced NLO properties, they have been identified as promising candidates for device applications [13-15]. Our research group are also concentrating on the development of NLO crystals [16,17]. Effort has been taken to synthesise and characterise the organic, inorganic and semi-organic crystals for NLO applications. We have reported a new crystal of 4-Methoxybenzylammonium nitrate [4]. As a continuation of our work in 4-methoxybenzylamine based halogen compounds, we reported another novel crystal 4MPMAB and deposited the crystallographic information file in the Cambridge Crystallographic Data Centre [CCDC Number: 1814132]. The 4MPMAB crystal consists of 4MBA ($C_8H_{12}NO^+$) cation and bromine (Br^-) anion linked by N—H---Br hydrogen bond resulting in an open framework architecture with hydrogen bonded ammonium groups and bromide anions situated in layers parallel to (011), separated by various hydrophobic layers with interlocked anisole groups. N—H---Br and C—H---Br interactions play a decisive role in the crystal packing of the title compound. The grown crystal belongs to the centrosymmetric crystal system. In 4MPMAB crystal structure, the protonated amino group (NH_3^+) compensates the negative charge of the halogen (Br^-) anion group. The Br^- donor, transfer a proton to the acceptor NH_3^+ , enhances the nonlinearity and serves as an excellent NLO material. 4MPMAB exhibit considerable NLO coefficients, large transmission, wide bandwidth, better thermal and mechanical stability. Hence it can be preferably used for NLO devices. High power laser materials are in great demand and are extensively used in several applications. On the contrary, new nonlinear optical crystals are currently being developed for limiting the high intense laser beam, more importantly for protecting human eyes and optical sensors. Attempts are on the way to find the suitable optical limiters which exhibit low threshold value to safeguard the optical devices from high-

intensity laser radiation. Optical limiters depend on irradiance related NLO properties. Moreover, an effective optical limiter should have a higher third-order susceptibility and low optical threshold value. [18-22]. The present article focuses on the critical study of the crystal structure, molecular structure confirmation, thermal, mechanical, linear, nonlinear and optical limiting behaviour of the grown crystal. Furthermore, the relationship between the structure and property is also investigated.

2 Experimental methods

2.1 crystal growth

4MPMAB crystals were successfully synthesised by dissolving 4-methoxybenzylamine and hydrobromic acid (HBr) solution in the stoichiometric ratio of 1:1 in double distilled water, according to the following equation:



Scheme. 1 Reaction scheme of 4MPMAB crystal

The resultant solution was stirred well for more than 2h by a magnetic stirrer until it reached a homogeneous equilibrium. The mixture was then filtered by Whatman filter paper to remove the impurities. The final solution was kept in a constant temperature bath at 37 °C with ± 0.1 °C accuracy to control the rate of evaporation. Good colourless crystals suitable

for analysis were obtained in 5 weeks. The reaction scheme of 4MPMAB crystal is exhibited in scheme. 1. The photograph of the as-grown single crystal of 4MPMAB is shown in Fig. 1.

Fig. 1. As grown single crystal of 4MPMAB

2.2 Characterization techniques

Various characterisation methods were performed for the 4MPMAB crystal to investigate the suitability for device applications. A single crystal was used for X-ray measurements, with a Bruker AXS Kappa Apex2 CMOS diffractometer operating at 296 K with the wavelength $\text{MoK}\alpha = 0.71073\text{\AA}$. A colourless crystal of 4MPMAB with size $0.25 \times 0.23 \times 0.20$ mm was selected for the data collection. For the title compound, data collection: APEX2 [23] cell refinement: SAINT [23]; data reduction: SAINT [23]; program (s) was used to solve structure: SHELXT 2014/5 [24]; program (s) was used to refine structure SHELXL-2018/1 [25]; molecular graphics: ORTEP-3 for Windows [26] and PLATON [27]; software used to prepare material for publication: SHELXL2018/1 [25] and PLATON [27]. All non hydrogen atoms were refined anisotropically. All H atoms were located in a difference Fourier map, but were repositioned geometrically and as riding, with C—H distances of 0.93 (aromatic), 0.97 (methylene) or 0.96 Å (methyl) and N—H distances of 0.89 Å. The torsion angles of the methyl and ammonium H atoms were allowed to refine to best fit the experimental electron density map and the U_{iso} (H) values of these groups were constrained to 1.5 times that of their carrier atom. For the other hydrogen atoms, U_{iso} was set to 1.2 times U_{eq} of the carrier atom. The CIF file is provided in supplementary information. The details of crystal data and the structural refinement for 4MPMAB crystal are summarised in Table. 1.

Powder X-ray diffraction was done using pan analytical XPERT-PRO X-ray diffractometer with Cu $\text{K}\alpha$ ($\lambda = 1.54060$ Å) radiation to assess the crystalline quality and to

index the diffraction peaks. The sample was scrutinised in the 2θ values range between 10.0231° and 80.9231° with step size $0.05^\circ/s$ at a rate of 10.1600s. The FT-IR spectrum was recorded with the help of KBR pellet method in the wavenumber region between 400 and 4000 cm^{-1} using BRUKER spectrophotometer to confirm the functional groups and the vibrational modes. The ^1H NMR and ^{13}C NMR spectrum were recorded for the grown crystal at 300 MHz using a BRUKER AMX spectrometer in DMSO solvent to verify the presence of hydrogen and carbon environment. Thermogravimetric analysis was performed to know the thermal stability using SDTQ 600 simultaneous thermogravimetric analyser in a nitrogen gas atmosphere between 25°C and 1000°C with a heating rate of $20^\circ\text{C}/\text{min}$. 4MPMAB crystal was subjected to Vicker's indentation study using SHIMADZU diamond pyramidal indenter to analyse the mechanical nature of the crystal. The optical transmittance is investigated by UV-Vis-NIR transmission spectrum recorded in Perkin Elmer spectrophotometer in the range of 190-1100 nm, and the bandgap is determined from the Tauc's plot. The Z-scan method was carried out to determine the nonlinear refractive index (n_2), the nonlinear absorption coefficient (β), nonlinear susceptibility (χ^3) using a continuous wave diode pumped 532 nm Nd:YAG laser beam of power 50 mW, focused with a lens measures 3.5 cm focal length. The optical limiting experiment was performed using the same exciting source adopted in the Z-scan study to know the threshold wavelength of the grown sample.

3. Results and discussion

3.1 Single crystal XRD analysis

The crystal 4MPMAB, crystallises in centrosymmetric monoclinic space group $P2_1/c$, with $Z = 4$, having one independent cation and an anion in the asymmetric unit. The atomic numbering scheme of the crystal is illustrated in Fig. 2. (C1-C8/O1) atoms form a mean plane with an r.m.s. deviation of 0.0294 \AA . The N1 atom deviates away from this mean

plane by 1.3411 (31) Å. The network of ammonium and bromide ions are linked by N—H---Br hydrogen bonds. The crystal packing diagram viewed along the *a* axis is exhibited in Fig. 3. The cations and anions are connected by C—H---Br and N—H---Br hydrogen bonds. The fluctuation in the N---Br distances [3.291 (2) to 3.312 (2) Å], reveals strong bonding between the ions of ammonium and halogenide ions [28]. The organic fragments are found between consecutive inorganic layers. The combination of bromide ions and ammonium groups which are parallel to the *bc* plane possesses numerous hydrogen bonds that bridge distinct entities of the compound to form inorganic layers Fig. 3. The different graph-set motifs which includes $R_2^4(8)$ and $R_2^8(16)$ motifs are noticeable inside the layers [29]. The organic fragments are found between consecutive inorganic layers Fig. 4. π - π stacking interactions are not observed between the phenylene rings. C7—H7A... π interaction involving (C1—C6) benzene ring is noticed (Table. 2, Fig. 5.). The organic molecule reveals a constant dimensional configuration with habitual distances and angles. The C1—O1 [1.359 (3) Å] distance is marginally lesser than that of C8—O1 distance [1.432 (3) Å], which can be ascribed to the donor mesomeric effect of the methoxy group. All the geometrical characteristics of the crystal accord with the features of the related compound [28].

Fig. 2. A view of the asymmetric unit in (I) showing atom numbering and ellipsoids drawn at the 40% probability level. Dashed lines indicate hydrogen bonding interaction.

Fig. 3. Projection along the *a* axis of the inorganic layer in the structure of the title compound, showing the N—H...Br hydrogen bonding interactions (dashed lines). Only the ammonium and bromide sections are shown for clarity.

Fig. 4. Projection of the structure of the title compound along the *b* axis, Hydrogen bonds are shown as thin black dashed lines.

Fig. 5. Partial packing showing the C7—H7A $\cdots\pi$ interactions involving (C1—C6) benzene ring.

Table 1. Crystal data and structure refinement for 4MPMAB crystal

Table 2. Hydrogen-bond geometry (Å, °)

3.2 Powder XRD study

The PXRD analysis confirms the crystalline nature and the crystal system of the grown crystals. The sharp and high-intensity diffraction peaks seen in the PXRD diffractogram (Fig. 6) evidences the better crystalline quality of 4MPMAB crystal [30]. The diffraction peaks have been indexed by using the *indx* software. The lattice parameters are determined by unit cell software. The calculated lattice parameters are in good agreement with the experimental data obtained from the single crystal X-ray data. The unit cell values determined from single crystal XRD analysis and powder XRD analysis are compared in table 3. For photonic device fabrication, good crystal with perfect crystalline quality is required as they rely on the transmission of light and eliminates the scattering of light [31]. As 4MPMAB possess better crystalline property, it can be a suitable material for photonic applications.

Fig. 6. Powder XRD diffractogram of 4MPMAB crystal

Table 3. Comparison of single crystal and powder XRD values of 4MPMAB crystal

3.3 Vibrational spectroscopic measurement:

3.3.1 FT-IR Spectral study

The crystal structure has various functional groups such as NH_3^+ , CH_3 , CH_2 , C-N, C-C, C-O and C-H. The vibrational assignments and corresponding wave numbers are

summarised in the table. 4. The FT-IR spectrum of 4MPMAB is shown in Fig. 7. The broadband noticed between 3450-2700 cm^{-1} in FT-IR is due to the N-H, C-H stretching mode and N—H---Br intermolecular hydrogen bond. The sharp and medium intensity bands at 2698, 2596 cm^{-1} are evident for the N—H---Br intermolecular interactions. The N—H---Br intermolecular hydrogen bonds play a significant role in stabilising the crystal structure. The medium intensity peaks at 1607 is assigned for NH_3^+ symmetric bending vibration, which confirms the formation of NH_3^+ moiety due to the protonation of NH_2 through N—H---Br interaction. C-C ring stretching mode corresponds to 1460 cm^{-1} and 1514 cm^{-1} . The peak appeared at 1373 cm^{-1} is assigned to CH_3 symmetric deformation mode. C-N stretching vibration is appeared at 1301 cm^{-1} . The intense C-O-C asymmetric stretching vibration peak is observed at 1254 cm^{-1} . The bands at 1117, 1079, 1022 cm^{-1} are attributed to the C-H in-plane deformation mode. At 950 cm^{-1} , medium intensity peak is ascribed to C-H out of plane bending mode. CH_2 rocking mode is observed at 832 cm^{-1} . The weak peaks appeared at 738 cm^{-1} and 711 cm^{-1} are assigned as C-H out of plane deformation. The bands observed from 636 to 457 cm^{-1} are assigned to C-C-C bending mode [32-37]. The halogen ligand coordination confirms the existence of 4MPMAB compound. Furthermore, the crystal structure is revealed through protonation and the N—H---Br influence is also evidenced.

Fig. 7. FT-IR spectrum of 4MPMAB crystal

Table 4. Vibrational assignments of 4MPMAB crystal

3.4 NMR spectral analysis

3.4.1 ^1H NMR spectral analysis

The ^1H NMR spectrum detects the presence of protons and the number of hydrogen nuclei coupled to that group. The position of hydrogen atom in the organic ligand is shown in

Fig. 8. The resonating signal of 4MPMAB is compared with the ^1H NMR signal of 4MBA [38] in table 5. The expected five different proton signals are observed in the spectrum (Fig. 9.) DMSO water peak is observed at 3.406 ppm and the solvent signal appears at 2.505 ppm [39]. The two adjacent doublet proton signals at 7.419 ppm (A), 7.390 ppm (A) and 6.989 ppm (B), 6.960 ppm (B) are attributed to the aromatic ring protons. The resonating shift of aromatic carbon signals compared to 4MBA may be due to the C7—H7A---Cg1⁽ⁱⁱⁱ⁾ interaction. In 4MBA, the methylene proton signal is noticed at 3.77 ppm (C). This signal is shifted and a multiplet is seen in 4MPMAB crystal between 3.989 and 3.933 ppm due to C—H---Br and N—H---Br hydrogen bond interactions. The methyl proton is observed at 3.758 ppm (D) in 4MPMAB crystal. The NH_2 proton peak of 4MBA observed at 1.41 ppm is absent in 4MPMAB crystal. The presence of a signal at 8.143 ppm (E) corresponds to the protonated amino moiety (NH_3^+). A proton from HBr is transferred to NH_2 group of 4MBA. Here the NH_3 group is coordinated with Br^- through N—H---Br bonds. This further supplements the FT-IR observation and confirms the formation of the 4MPMAB crystal.

Fig. 8. The position of hydrogen atom in the organic part of the 4MPMAB crystal

Table 5. Comparison of ^1H NMR resonating signal of 4MBA with 4MPMAB crystal

Fig. 9. ^1H NMR spectrum of 4MPMAB crystal

3.4.2 ^{13}C NMR spectral analysis

The ^{13}C NMR spectral study detects the presence of carbon in aromatic, methyl and methylene groups respectively. The position of carbon atom in the titled crystal is shown in Fig. 2. The 4MPMAB spectrum of ^{13}C NMR is presented in Fig. 10. The spectrum shows the six carbon signals. The ^{13}C NMR resonating signal of the 4MPMAB crystal is compared with the signal of 4MBA in the table. 6. The DMSO solvent peak is noticed between 39.11 and 40.78 ppm respectively. The resonance signal at 158.49, 135.67, 128.20 and 113.86 ppm are

due to the aromatic carbon of 4MBA which appear at 159.82 ppm (C₁), 131.06 ppm (C₄), 126.24 ppm (C₃, C₅) and 114.39 ppm (C₂, C₆) in 4MPMAB crystal. These shifts are due to C7—H7A...Cg1⁽ⁱⁱⁱ⁾ interaction. The upfield shifts of C₃, C₄, C₅ aromatic carbon signals are more pronounced than the other aromatic carbon signals as they are situated adjacent to the protonated amino moiety. The methylene peak of 4MBA is observed at 45.87 ppm. The corresponding peak is upfield shifted and appears at 42.11 ppm (C7) in the 4MPMAB crystal. The upfield shift is due to C7—H7B...Br1⁽ⁱ⁾, C7—H7A...Cg1⁽ⁱⁱⁱ⁾ and various N—H...Br interactions involved in the crystal. In addition to that, the upfield shift confirms the protonation of NH₂ by the hydrogen of H⁺ present in HBr. The signal at 55.75 ppm corresponds to the carbon attached to the methyl group of 4MBA, whereas the same peak is observed at 55.71 ppm (C8) in 4MPMAB crystal. This slight variation in the shift corresponds to the influence of C8—H8B...Br1⁽ⁱⁱ⁾ hydrogen bond. Thus the impact of hydrogen bond interactions are elucidated, and the formation of molecular structure is confirmed.

Fig. 10. ¹³C NMR spectrum of 4MPMAB crystal

Table 6. Comparison of ¹³C NMR resonating signal of 4MBA with 4MPMAB crystal

3.5 Thermal investigation

TG/DTA analysis assess the thermal nature of 4MPMAB crystal, and the TG/DTA plot is illustrated in Fig. 11. The initial weight of 6.0080 mg was taken for analysis. Decomposition is not observed up to the melting point of the crystal (219 °C). Hence it is understood that, no adsorbed water molecules present in the crystal [40]. This evidences the relative thermal stability of 4MPMAB till 219 °C. The first endothermic peak at 219 °C indicates the simultaneous melting and decomposition of 4MPMAB crystal. This confirms that 4MPMAB is well suitable for NLO applications until 219 °C. The TGA curve shows the

two-step decomposition process. Steady weight loss of about 40% is observed between 219 °C and 366 °C with corresponding endothermic peaks at 219 °C, 297 °C and 380 °C. This mass loss may be due to the decomposition of the organic moiety. Kefi et al. observed the similar melting point for poly (bis 4-methoxybenzylammonium)tetra- μ -chlorido-cadmate (II) crystal [32]. The second stage of degradation continues upto 650 °C. This corresponds to the liberation of the inorganic moiety. Finally, 23.14 % (1.390 mg) of initial weight was retained.

Fig. 11. TGA/DTA plot of 4MPMAB crystal

3.6 Mechanical study

Mechanical property needs to be assessed for utilising the crystal for NLO application. Vicker's indentation test is carried out to reveal the mechanical stability of 4MPMAB crystal. Fig. 12 depicts the variation of hardness number (H_v) with different load. Each hardness value (H_v) represents the average value of the diagonal length of various indentations. The Vicker's hardness values were determined by the standard relation.

$$H_v = 1.8544X\left(\frac{P}{d^2}\right)Kg / mm^2 \quad (1)$$

where P is the load in Kg and d is the average diagonal length in mm.

The value of hardness linearly rises with an increase in load from 5g to 50g then H_v is found to be gradually nearing the saturation point. At 100g, it almost reaches the saturation. Hence 4MPMAB crystal realises the reverse indentation size effect (RISE). The log P vs log d plot is illustrated in Fig. 13. Work hardening coefficient (n) is assessed from the slope of Fig. 13. The n value is determined to be 4.1, which is higher than 2, reveals the soft nature of 4MPMAB crystal [41].

Fig. 12. Variation of hardness number on applied indentation load of 4MPMAB crystal

Fig. 13. The plot of log P vs log d of 4MPMAB crystal

3.7 Optical studies

3.7.1 Linear optical study

The transmission spectrum displayed in Fig. 14. shows the lower cut-off wavelength at 330 nm. 4MPMAB crystal is said to exhibit π - π^* transition [42]. 4MPMAB has a wide optical window from 330 nm to 1200 nm, which is an essential criterion for NLO application. The UV-Vis-NIR transmission spectrum shows good transmittance percentage of about 65%, which indicates the transparent nature and enables the crystal for NLO applications. The transmittance (T) of 4MPMAB crystal is used to determine the absorption coefficient (α) using the relation,

$$\alpha = \frac{2.3026 \log(1/T)}{t} \quad (2)$$

The relation between optical bandgap (E_g), absorption coefficient (α) and photon energy ($h\nu$) of 4MPMAB crystal is given by,

$$(\alpha h\nu)^2 = B(h\nu - E_g) \quad (3)$$

The bandgap value can be calculated from the Tauc's plot (Fig. 15) between $(\alpha h\nu)^2$ and $h\nu$. The linear part is extrapolated and intercepted in X coordinate, and the bandgap value is found to be 3.5 eV. This wide bandgap and the optical transparency of the crystal is especially suited for LED and laser diodes in the field of optoelectronics [43].

Fig. 14. Transmission spectrum of 4MPMAB crystal**Fig. 15.** Tauc's plot of 4MPMAB crystal

3.7.2 Third-order nonlinear optical study

The third order nonlinearity at a specified wavelength has been studied to utilise the title crystal for NLO applications. The third-order properties of 4MPMAB were investigated by a simple and accurate Z-scan technique employed by Bahae et al [44]. The laser beam was incident normally on the sample through a lens and the sample was moved through the axial direction from +Z to -Z. The nonlinear refractive index produces a change in focusing and defocusing of the light depending on the positive and negative value of n_2 . The sample is placed at the far field concerning the position of the sample to find the phase shift. For an open aperture, the aperture is removed, and the entire transmitted beam is collected and the intensity absorption is determined. The transmitted intensity was measured by a detector attached by a digital power meter at the closed aperture (Fig. 16) and open aperture (Fig. 17) configuration. The closed aperture transmittance depends on both nonlinear refractive index and nonlinear absorption. The open aperture transmittance depends only on nonlinear absorption. The closed aperture data should be divided by corresponding open aperture data to obtain the pure refractive index [45]. The ratio of closed to open aperture Z scan curve is shown in (Fig. 18). The peak to valley pattern of closed aperture curve demonstrates the self-defocusing nature, because of the negative nonlinearity of 4MPMAB crystal. Henceforth the crystal can be used for optical sensors [46]. The maximum transmission is observed near the focus ($Z=0$) which corresponds to the saturable absorption of 4MPMAB. This property can be utilised in laser applications such as picosecond pulse shapers and mode lockers [47]. The third-order nonlinear parameters calculated using standard relations [48] are displayed in table 7. The third-order nonlinear susceptibility χ^3 value of 4MPMAB crystal is larger when compared with other well-known crystals and is tabulated in the table. 8 [18,49]. In 4MPMAB, HBr transfers a proton to the amine group (NH_2) of organic ligand and forms an

amino moiety (NH_3^+). A strong intermolecular hydrogen bond N—H---Br is formed between NH_3^+ cation and Br^- anion. This improves the charge transfer and results in larger hyperpolarisation and encourages higher third-order nonlinearity. Consequently, the 4MPMAB crystal is endorsed as an efficient material for NLO devices.

Fig. 16. Closed aperture Z-scan curve of the 4MPMAB crystal

Fig. 17. Open aperture Z-scan curve of the 4MPMAB crystal

Fig. 18. The ratio of open to closed aperture Z-scan curve of the 4MPMAB crystal

Table 7. Third order nonlinear optical parameters of 4MPMAB crystal

Table 8. $\chi^{(3)}$ values of several representative nonlinear crystals

3.7.3 Optical limiting behaviour

The optical limiting behaviour of the grown crystal was analysed using the Z-scan technique by placing the crystal in the valley point. The input power is varied systematically and the corresponding output power is detected by a power meter. A graph is plotted between the input power along the X-axis and the output power along the Y-axis. The optical limiting curve is illustrated in Fig. 19. From the curve, it is obvious that the output transmittance power increases with increasing input power and obey's Beer-Lambert's law. On further increasing the input power, the output power reaches the plateau and attains saturation and becomes nonlinear [50]. The maximum output power shows threshold limiting amplitude at 24.3 mW and qualifies the crystal for passive optical limiting devices to compensate the fluctuating signal in telecommunication applications [18].

Fig. 19. The optical limiting curve of 4MPMAB crystal

4 Conclusion

In summary, we accomplished in developing a new organic halogen bonded crystal, 4MPMAB for third harmonic generation of the laser frequency. The crystal belongs to the monoclinic system. The PXRD analysis assessed the crystalline perfection. The crystal shows the donor mesomeric effect. The crystal packing of 4MPMAB is determined by N—H---Br and C—H---Br interactions. The single crystal XRD and PXRD study strongly support the validation of the 4MPMAB structure. In addition to that, FT-IR, ^1H NMR, ^{13}C NMR, results were consistent with structural components determined by single crystal XRD study. The influence of intermolecular hydrogen bonding interactions of the crystal packing and the protonation is recognised. It is worthy to note that 4MPMAB is thermally stable upto 219 °C. soft nature of the grown crystal is revealed. The UV-Vis-NIR spectrum shows the maximum transmission from 330 nm to 1100 nm and has the optical band gap of 3.5 eV. The Z-scan study reveals that 4MPMAB exhibits good third-order NLO properties, due to the transfer of protons between the organic cation and halogen anion and hydrogen bond interactions. The relationship between structure and third order NLO properties were well established. These properties reveal the potential application of 4MPMAB toward photonic devices. Moreover, 4MPMAB crystal shows a better optical limiting response at 532 nm for optical limiting applications.

Acknowledgement

The authors are thankful to the School of Pure and Applied Physics - MG University, Kottayam, Kerala for the single crystal XRD data, CECRI, Karaikudi for powder XRD analysis, St. Joseph's College (Autonomous), Tiruchirappalli for providing UV-Vis-NIR, FT-IR spectra, SASTRA university, Thanjavur for recording NMR spectra and TG/DTA analysis, National college, Tiruchirappalli for microhardness study and to Dr. Vinita, VIT, Chennai for Z scan analysis.

References

- [1] A. Anbarasi, S.M.R. Kumar, G.J.S. Sundar, M. A. Mosses, M. Packiyaraj, M. Prabhakaran, R. Ravisankar, R. Gunaseelan, *Physica B*, (2017) doi:10.1016/j.physb.2017.06.089.
- [2] A. Subashini, S. Leela, K. Ramamoorthi, A. Arakcheeva, H. Stoeckli-evans, G. Chapuis V. Petr, P. Pattison, P. Reji, *CrystEngComm*. 15 (2013) 2474–2481.
- [3] R. Surekha, R. Gunaseelan, P. Sagayaraj, K. Ambujam, *CrystEngComm*. 16 (2014) 7979–7989.
- [4] C.T. Chen, G.Z. Liu, *Ann. Rev. Mater. Sci*, 16 (1986) 203-243.
- [5] Y. Fei, B.H.T. Chai, C.A. Ebberts, Z.M. Liao, K.I. Schaffers, P. Thelin, *J. Cryst. Growth*. 290 (2006) 301–306.
- [6] M.D. Zidan, M.M. Al-Ktaifani, A. Allahham, *Opt. Laser Technol*. 90 (2017) 174–178.
- [7] M.K. Kumar, S. Sudhakar, P. Pandi, G. Bhagavannarayana, R.M. Kumar, *Opt. Mater*. 36 (2014) 988–995.
- [8] J. Jeyaram, K. Varadharajan, B. Singaram, R. Rajendhran, *J. Cryst. Growth*. (2018). doi:10.1016/j.jcrysgro.2018.01.015.
- [9] V. Singh, P. Aghamkar, *Applied optics*. 51 (2012) 2288-2297.
- [10] C. Videlot-ackermann, T. Isoshima, A. Yassar, T. Wada, H. Sasabe, D. Fichou, *J. Synthmet*. 156 (2006) 154–161.
- [11] R. Thomas, S. Pal, A. Datta, M.K. Marchewka, H. Ratajczak, S. Pati, G.U. Kulkarni, *J. Chem.Sci*. 120, (2008) 613-620.
- [12] P.S.L. Mageshwari, R. Priya, S. Krishnan, V. Joseph, S.J. Das, *Opt. Laser Technol*. 85 (2016) 66–74.
- [13] N. Mahbouli Rhouma, A. Rayes, F. Mezzadri, G. Calestani, M. Loukil, *Acta Cryst E*. 72 (2016) 1050–1053.
- [14] P. Umarani, A. Thiruvalluvar, C. R Raja, *IUCrData*. 2 (2017) x171114.
- [15] J.T. Yang, S.J. Luo, L. Yi, *Physica B*. 408 (2013) 175–182.
- [16] A.N. Vigneshwaran, P. Umarani, C.R. Raja, *J. Mater. Sci. Mater. Electron*. 28 (2017) 11430–11438.
- [17] A.N. Vigneshwaran, A.A. Joseph, C.R. Raja, *Optik*. 127 (2016) 5365–5369.
- [18] A. Sundari, S. Manikandan, *J. Mater. Sci. Mater. Electron*. 29 (2018) 558-567.

- [19] T.C.S. Girisun, S. Dhanuskodi, G. Vinitha, *Mater. Chem. Phys.* 129 (2011) 9–14.
- [20] R. Gomathi, S. Madeswaran, D.R. Babu, *Mater. Chem. Phys.* 207 (2018) 84–90.
- [21] C. Ramki, R.E. Vizhi, *Mater. Chem. Phys.* 205 (2018) 138-146.
- [22] S. Manikandan, T.C.S. Girisun, R. Mohandoss, S. Dhanuskodi, S. Manivannan, *Optics and Spectroscopy*. 117 (2014) 469–473.
- [23] Bruker. APEX2, SAINT and SADABS. BRUKER AXS Inc, Madison, Wisconsin, USA (2009).
- [24] G.M. Sheldrick, *Acta Cryst. A*71 (2015) 3-8.
- [25] G.M. Sheldrick, *Acta Cryst. C*71 (2015) 3-8.
- [26] L.J. Farrugia, *J. Appl. Cryst.* 45 (2012) 849-854.
- [27] A.L. Spek, *Acta Cryst. D*65 (2009) 148-155.
- [28] R. Kefi, Z. Matthias, C. Ben Nasr, *Acta Cryst. E*67 (2011) o634.
- [29] J. Bernstein, R.E. Davids, L. Shimoni, N.L. Chang, *Angew. Chem. Int. Ed. Engl.* 34 (1995) 1555-1573.
- [30] B. Dhanalakshmi, S. Ponnusamy, C. Muthamizhchelvan, V. Subashini, *J. Cryst. Growth*. 426 (2015) 103-109.
- [31] A. Krishna, Sonia, N. Vijayan, S. Verma, B. Singh, I. Bidkin, M.S. Jayalakshmy, B. Sridhar, S. Das, *J. Mater. Sci. Mater. Electron.* 28 (2017) 4306-4312.
- [32] R. Kefi, M. Zeller, F. Lefebvre, C. Ben Nasr, *Elixir Appl. Chem.* 43 (2012) 6701–6706.

- [33] R. Anitha, S. Athimoolam, M. Gunasekaran, *Spectrochim Acta A.* 138 (2015) 753-762
- [34] H.G. Brittain, *Cryst. Growth Des.* 11 (2011) 2500–2509.
- [35] A. Raj, K. Raju, H.T. Varghese, C.M. Granadeiro, H.I.S. Nogueira, C. Yohannan Panicker, *J. Braz. Chem. Soc.* 20 (2009) 549–559.
- [36] S. Gunasekaran, E. Sailatha, S. Seshadri, S. Kumaresan, *Indian J. Pure. Appl Phys.* 47 (2009) 12-18.
- [37] S. Mohan, A.R. Prabakaran, *Proc. Indian Natn. Sci. Acad.* 58 (1992) 269–274.
- [38] K. B. Gudasi, *J. react funct polym.* 66 (2006) 1149–1157.
- [39] S. Karthigha, S. Kalainathan, F. Hamada, M. Yamada², Y. Kondo, *RSC Adv.* 6 (2016) 33159-33169.
- [40] T. Thaila, S. Kumararaman, *Arch. Appl. Sci. Res.* 4 (2012)1494-1501.
- [41] K. Senthil, S. Kalainathan, F. Hamada , Y. Kondo, *RSC Adv.* 5 (2015) 79298-79308.
- [42] S. Pramodini, P. Poornesh, Y.N. Sudhakar, M.S. Kumar, *Opt. Commun.* 293 (2013) 125–132.
- [43] B. Periyasamy, R. Jebas, B. Thailampillai, *Mater. Lett.* 61 (2007) 1489-1491.
- [44] M. Sheik-bahae, A.A. Said, T.H. Wei, D.J. Hagan, E.W.V. Stryland, *IEEE J. Quantum. Electron.* 26 (1990) 760-769.
- [45] K. Senthil, S. Kalainathan, Y. Kondo, F. Hamada, M. Yamada, *Opt. Laser Technol.* 90 (2017) 242-251.
- [46] A. Subashini, R. Kumaravel, S. Leela, H.S. Evans, D. Sastikumar, K. Ramamurthi,

Spectrochim. Acta - Part A. 78 (2011) 935–941.

- [47] J. Sun, W. F. Guo, X. Q. Wang, G. H. Zhang, X. B. Sun, L.Y. Zhu, Q. Ren, D. Xu, Opt. Commun. 280 (2007) 183–187.
- [48] M. Nirosha, S. Kalainathan, S. Sarveswari, V. Vijayakumar, A. Srikanth, Spectrochim. Acta - Part A. 137 (2015) 23–28.
- [49] I. Md. Zahid, C. A. Kumar, A. Malarkodi, K. S. J. Wilson, R. M. Kumar, Mater. Lett. 209 (2017) 167-170.
- [50] T.C.S. Girisun, S. Dhanuskodi, D. Mangalraj, J. Phillip, Curr. Appl. Phys. 11 (2011) 838-843.

Table 1. Crystal data and structure refinement for 4MPMAB crystal

Empirical formula	C ₈ H ₁₂ Br N O
CCDC	1814132
Formula weight	218.10
Temperature	296(2) K
Wavelength	0.71073 Å
Crystal system	Monoclinic
Space group	P 2 ₁ /c
Unit cell dimensions	a = 11.6605(5) Å α = 90°. b = 9.2453(5) Å β = 105.472(2)°. c = 9.1907(5) Å γ = 90°.
Volume	954.90(8) Å ³
Z	4
Density (calculated)	1.517 Mg/m ³
Absorption coefficient	4.252 mm ⁻¹
F(000)	440
Crystal size	0.250 x 0.230 x 0.200 mm ³
Theta range for data collection	3.185 to 27.551°.
Index ranges	-15 ≤ h ≤ 15, -12 ≤ k ≤ 12, -11 ≤ l ≤ 11
Reflections collected	11559
Independent reflections	2187 [R(int) = 0.0439]
Completeness to theta = 25.000°	99.9 %
Absorption correction	Semi-empirical from equivalents
Max. and min. transmission	0.43 and 0.38
Refinement method	Full-matrix least-squares on F ²

Data / restraints / parameters	2187 / 0 / 102
Goodness-of-fit on F^2	1.092
Final R indices [$I > 2\sigma(I)$]	R1 = 0.0339, wR2 = 0.0666
R indices (all data)	R1 = 0.0524, wR2 = 0.0718
Extinction coefficient	n/a
Largest diff. peak and hole	0.287 and -0.550 e \AA^{-3}

Table 2. Hydrogen-bond geometry (Å, °)

D—H···A	D—H	H···A	D···A	D—H···A
C7—H7B···Br1 ⁽ⁱ⁾	0.97	3.06	3.918 (3)	148
C8—H8B···Br1 ⁽ⁱⁱ⁾	0.96	3.14	3.780 (3)	126
N1—H1A···Br1	0.89	2.41	3.291 (2)	174
N1—H1B···Br1 ⁽ⁱⁱⁱ⁾	0.89	2.41	3.300 (2)	175
N1—H1C···Br1 ^(iv)	0.89	2.44	3.312 (2)	168
C7—H7A···Cg1 ⁽ⁱⁱⁱ⁾	0.97	2.73	3.694 (3)	175

Cg1 is the centroid of benzene ring C1-C6

Symmetry codes: (i) $-x+1, -y+1, -z+1$; (ii) $x+1, y, z$;

(iii) $x, -y+1/2, z+1/2$; (iv) $-x+1, y-1/2, -z+1/2$

Table 3. Comparison of single crystal and powder XRD values of 4MPMAB crystal

Method	a (Å)	b (Å)	c (Å)	β°	Volume (Å ³)
Single crystal	11.6605 (5)	9.2453 (5)	9.1907 (5)	105.472(4)°	954.90 (8)
XRD					
Powder XRD	11.6596	9.2406	9.1806	105.693°	952.26

Table 4. Vibrational assignments of 4MPMAB crystal

Wave number cm^{-1}	Assignment
3450-2700	N-H, C-H stretching mode and N—H---Br intermolecular hydrogen bond
2791, 2698, 2596	N—H---Br intermolecular hydrogen bond
1607	NH_3^+ symmetric bending
1514, 1460	C-C ring stretching
1373	CH_3 symmetric deformation
1301	C-N stretching
1254	C-O-C asymmetric stretching
1117, 1079, 1022	C-H in plane deformation
950	C-H out of plane bending
832	CH_2 rocking
738, 711	C-H out of plane bending
636-457	C-C-C bending mode

Table 5. Comparison of ^1H NMR resonating signal of 4MBA with 4MPMAB crystal

Resonating signal of 4MBA in (ppm) [38]	Resonating signal of 4MPMAB in (ppm)	Functional group	Atom
7.254-7.126	7.419, 7.390	aromatic proton (CH)	A
6.920-6.793	6.989, 6.960	aromatic proton (CH)	B
3.77	3.989, 3.971, 3.952, 3.933	methylene proton (CH_2)	C
3.759	3.758	methyl proton (CH_3)	D
-	8.143	protonated amino moiety (NH_3^+)	E
1.41	-	Protons of amine (NH_2)	

Table 6. Comparison of ^{13}C NMR resonating signal of 4MBA with 4MPMAB crystal

Resonating signal of 4MBA in (ppm) [38]	Resonating signal of 4MPMAB in (ppm)	Functional group	Atom
158.49	159.82	aromatic carbon (CH)	C1
135.67	131.06	aromatic carbon (CH)	C4
128.20	126.24	aromatic carbon (CH)	C3,C5
113.86	114.39	aromatic carbon (CH)	C2, C6
45.87	42.11	methylene carbon (CH_2)	C7
55.15	55.71	methyl carbon (CH_3)	C8

Table 7. Third order nonlinear optical parameters of 4MPMAB crystal

Parameters	Values
Nonlinear refractive index (n_2)	$-8.44 \times 10^{-8} \text{ cm}^2/\text{W}$
Nonlinear absorption coefficient (β)	$0.01 \times 10^{-4} \text{ cm/W}$
Real part of susceptibility [$\text{Re } \chi^{(3)}$]	$3.36 \times 10^{-6} \text{ esu}$
Imaginary part of susceptibility [$\text{Im } \chi^{(3)}$]	$0.07 \times 10^{-6} \text{ esu}$
Third order susceptibility [$\chi^{(3)}$]	$3.36 \times 10^{-6} \text{ esu}$

Table 8. $\chi^{(3)}$ values of several representative nonlinear crystals

Crystal	Third order susceptibility $\chi^{(3)}$ (esu)
NaB5 [18]	2.07×10^{-7}
$\text{KBe}_2\text{BO}_3\text{F}_2$ [18]	0.99×10^{-13}
KDP [18]	2.04×10^{-14}
MMTC [49]	6.58×10^{-7}
VMST [49]	9.6963×10^{-12}
4MP4NP [49]	3.00844×10^{-7}
4MPMAB (present work)	6.21×10^{-6}

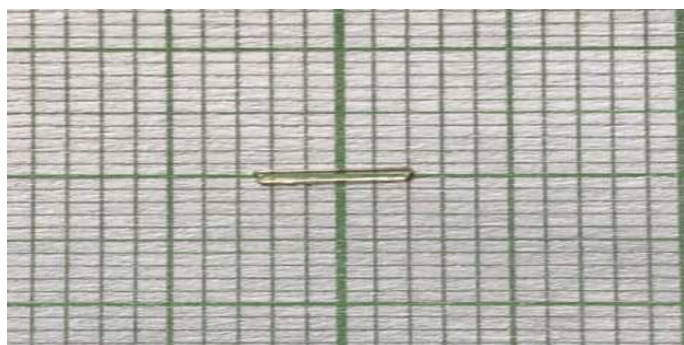


Fig. 1. As grown single crystal of 4MPMAB

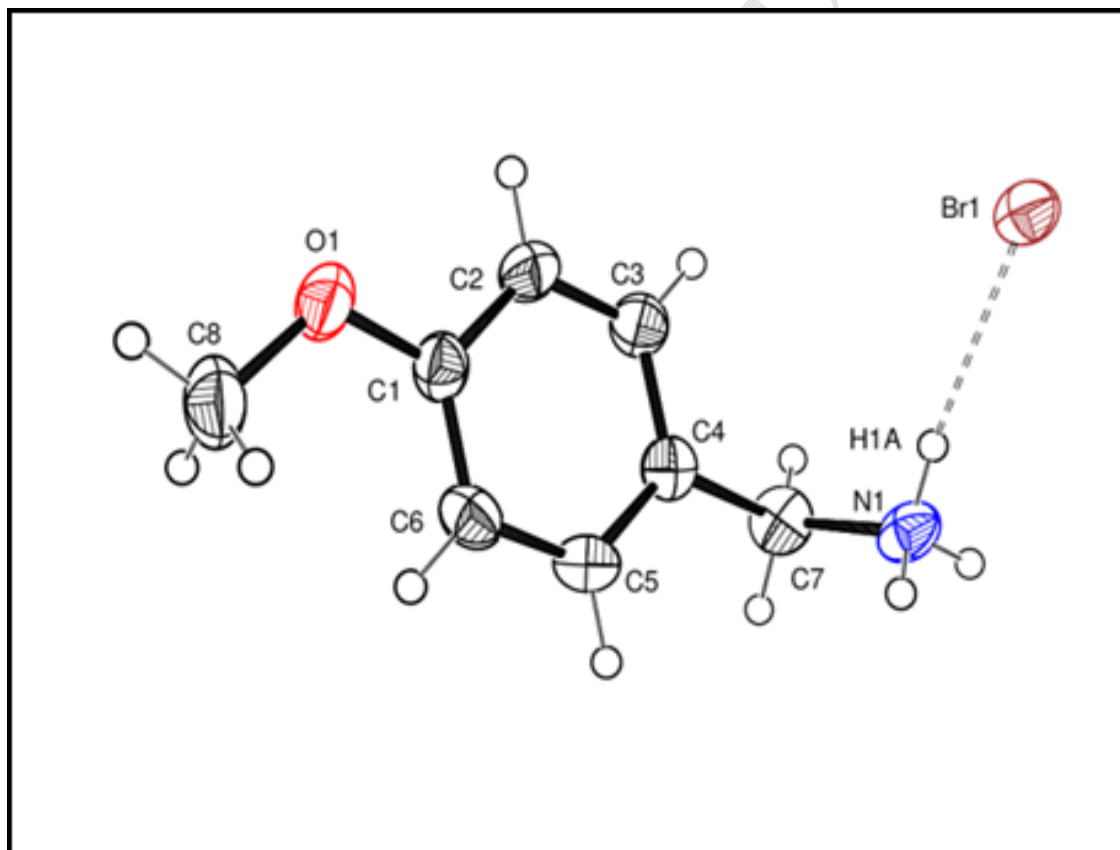


Fig. 2. A view of the asymmetric unit in (I) showing atom numbering and ellipsoids drawn at the 40% probability level. Dashed lines indicate hydrogen bonding interaction.

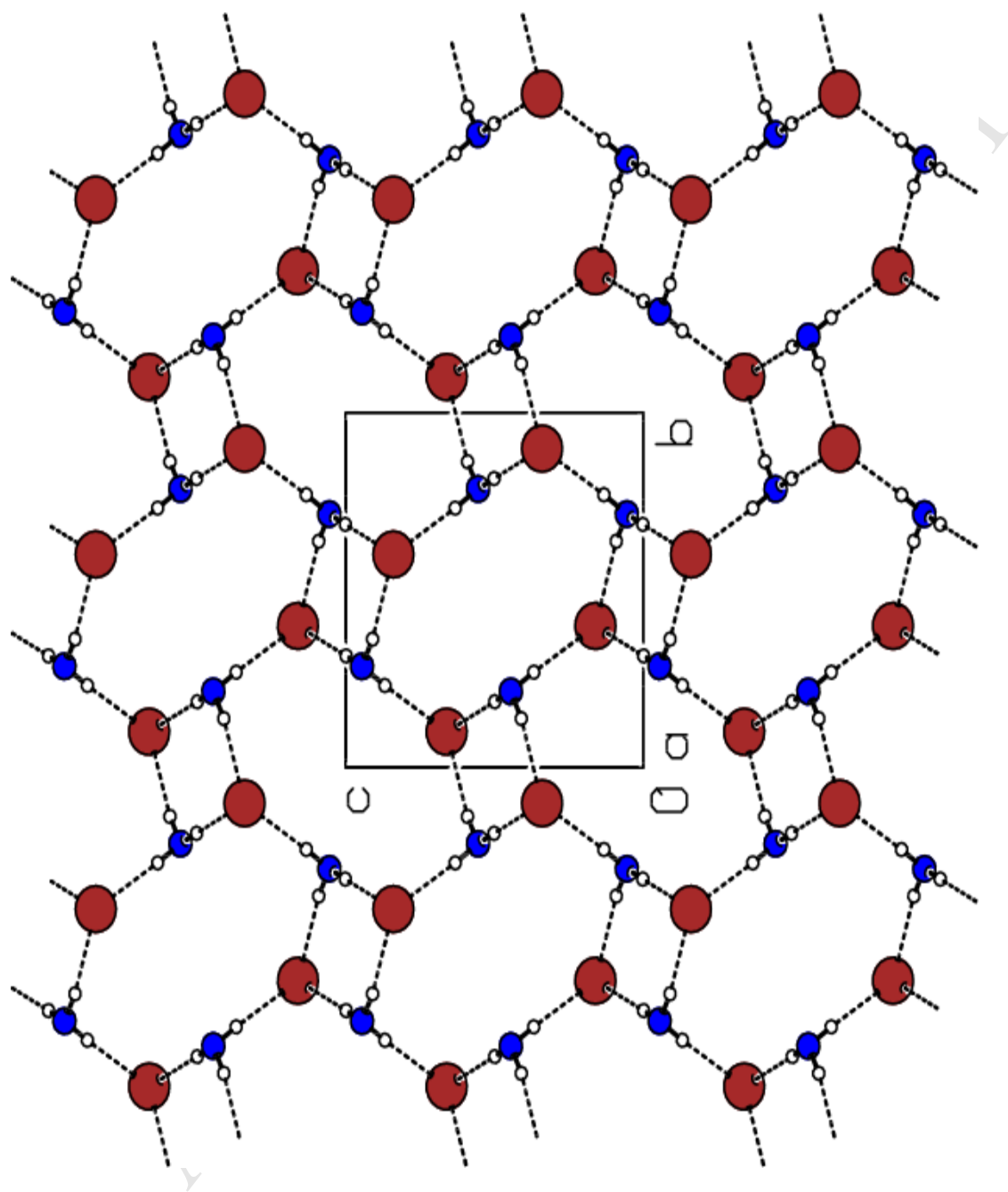


Fig. 3. Projection along the a axis of the inorganic layer in the structure of the title compound, showing the N—H \cdots Br hydrogen bonding interactions (dashed lines). Only the ammonium and bromide sections are shown for clarity.

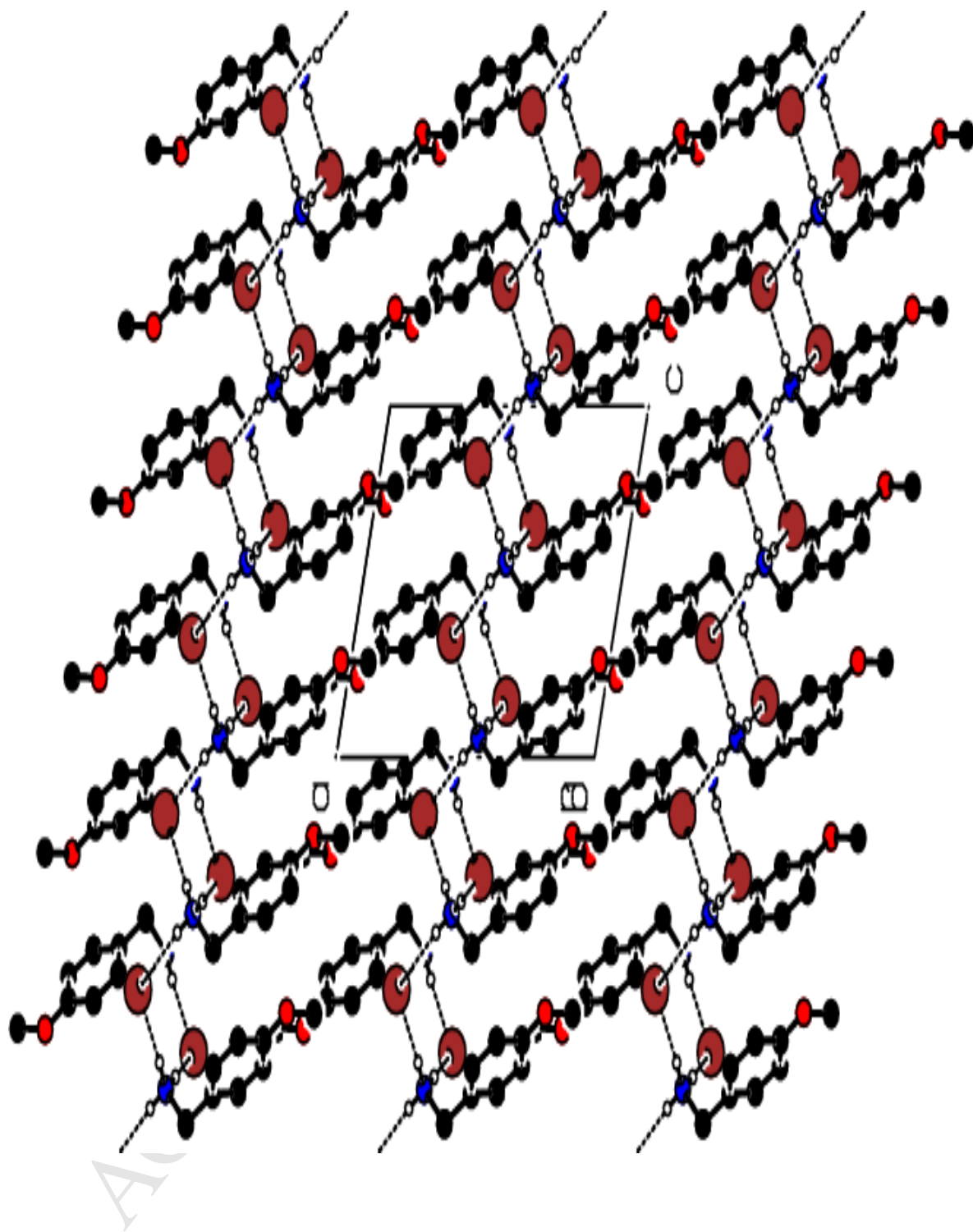


Fig. 4. Projection of the structure of the title compound along the b axis, hydrogen bonds are shown as thin black dashed lines.

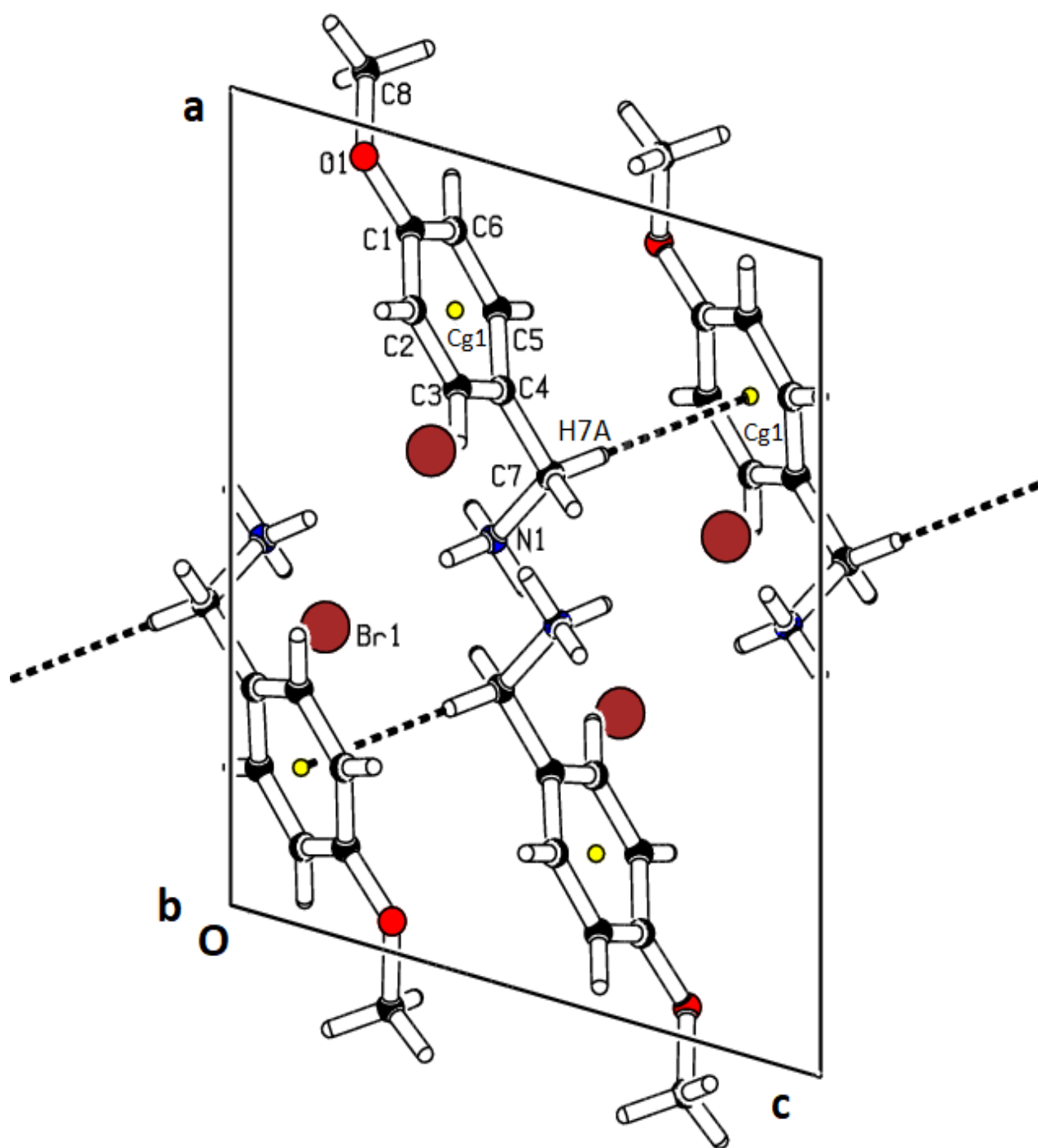


Fig. 5. Partial packing showing the C7—H7A $\cdots\pi$ interactions involving (C1—C6) benzene ring.

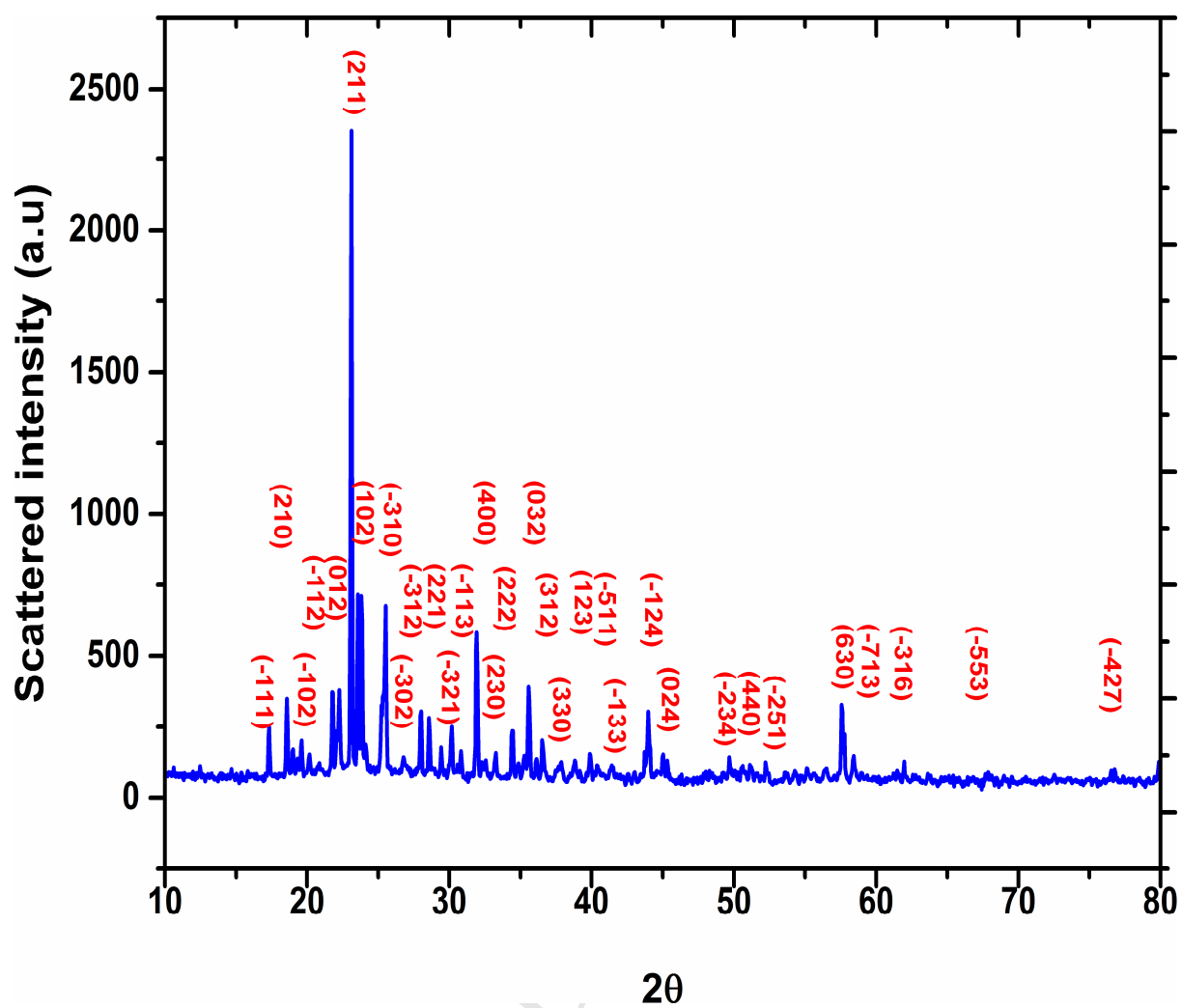


Fig. 6. Powder XRD diffractogram of 4MPMAB crystal

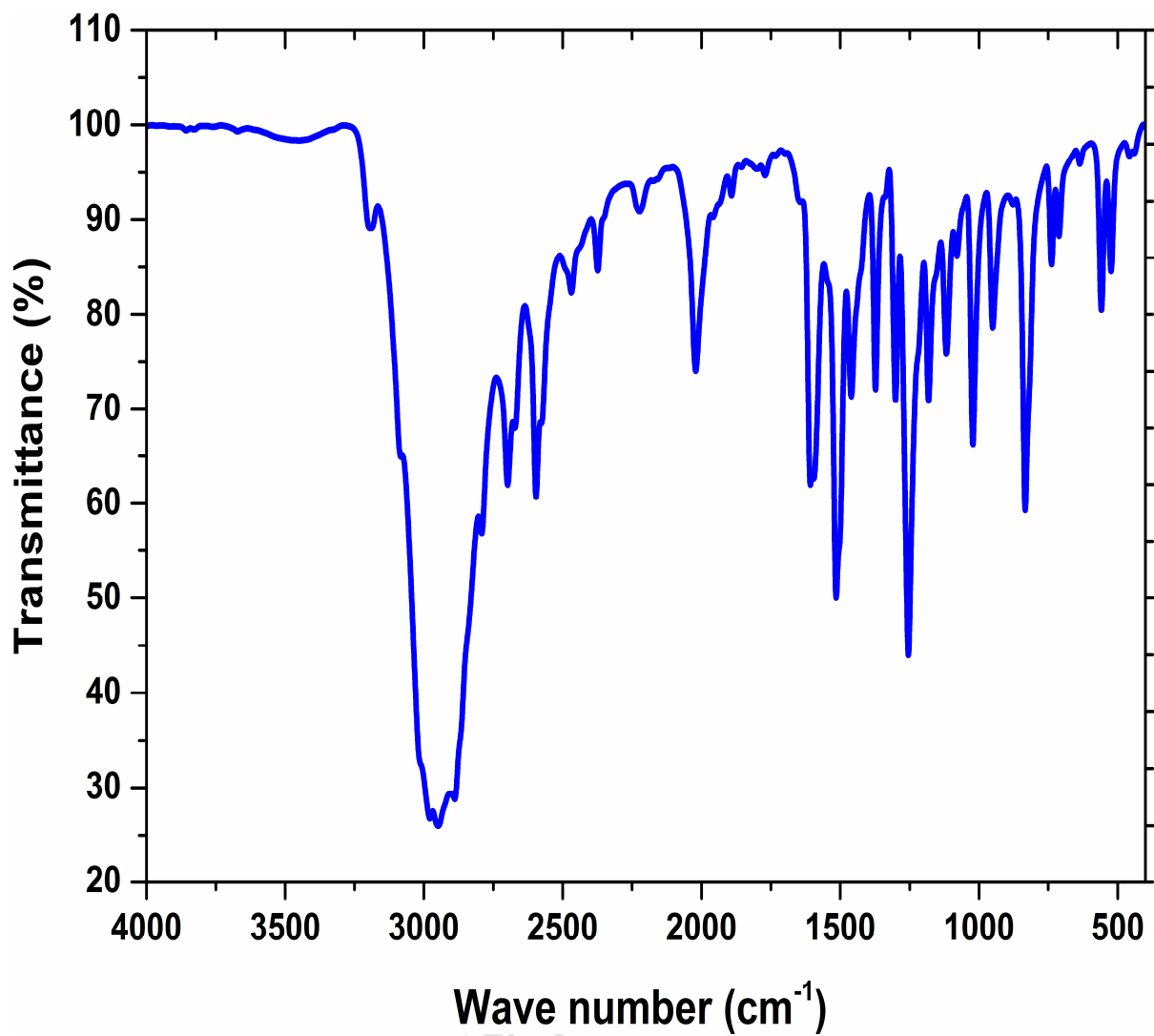


Fig. 7. FT-IR spectrum of 4MPMAB crystal

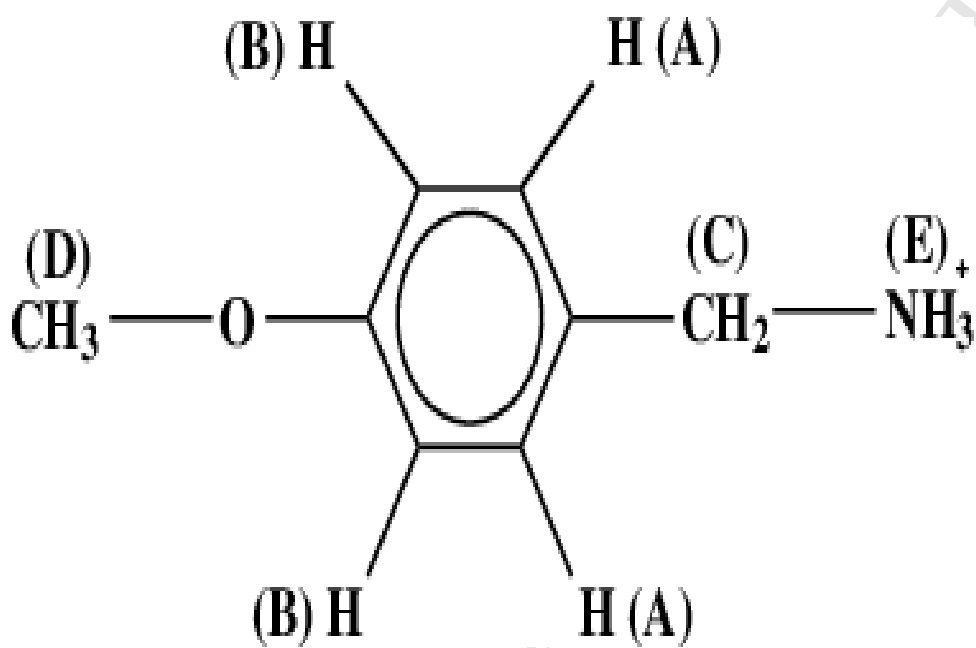


Fig. 8. The position of hydrogen atom in the organic part of the 4MPMAB crystal

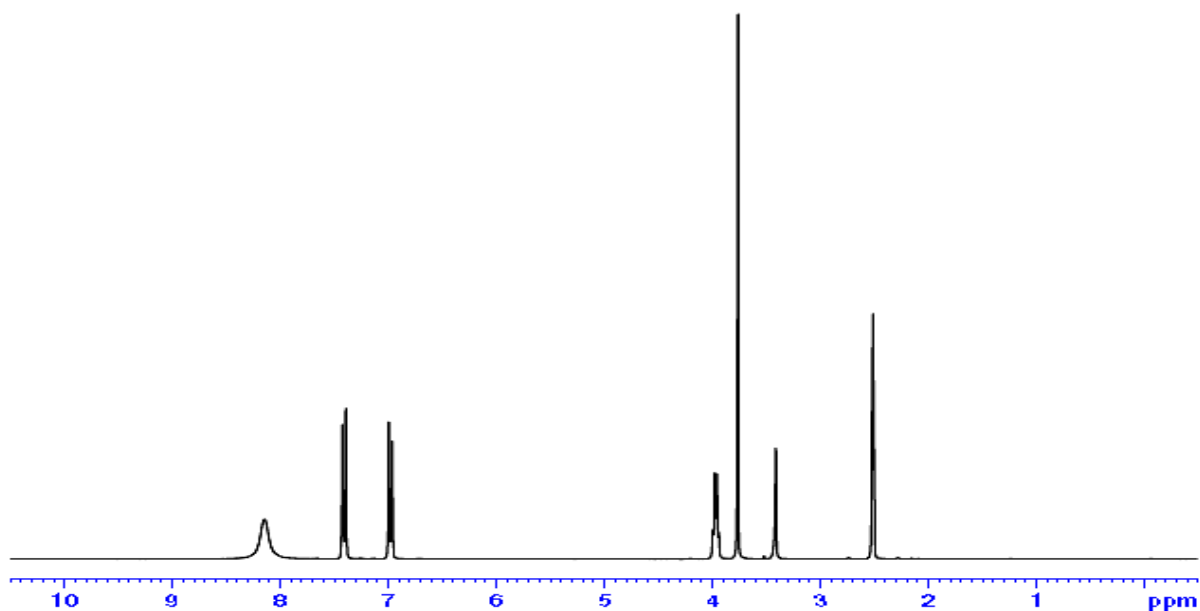


Fig. 9. ^1H NMR spectrum of 4MPMAB crystal

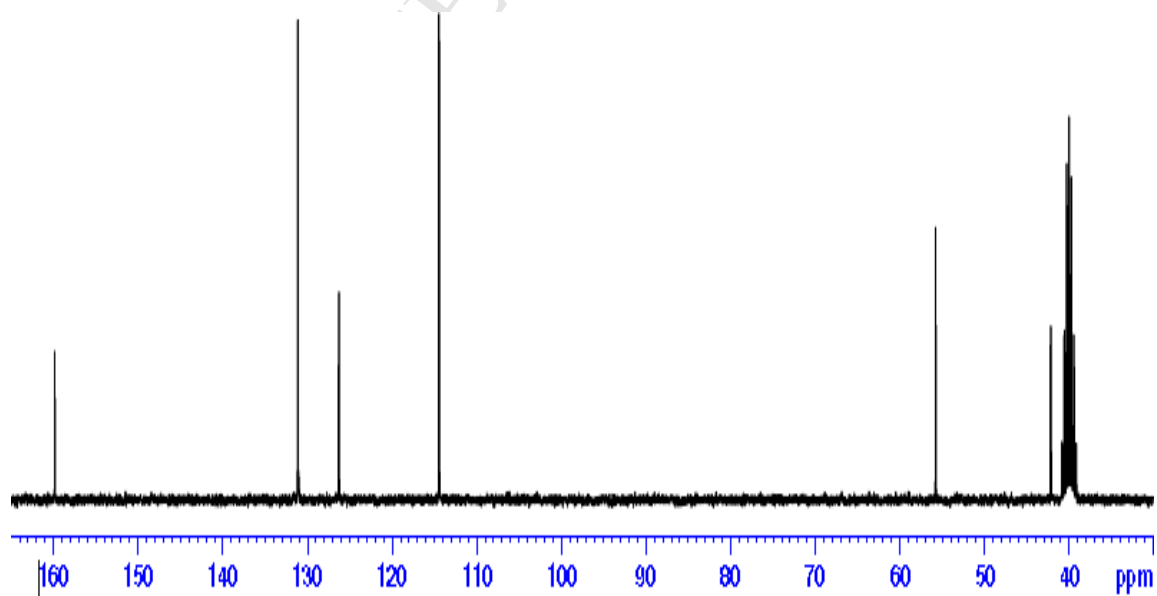


Fig. 10. ^{13}C NMR spectrum of 4MPMAB crystal

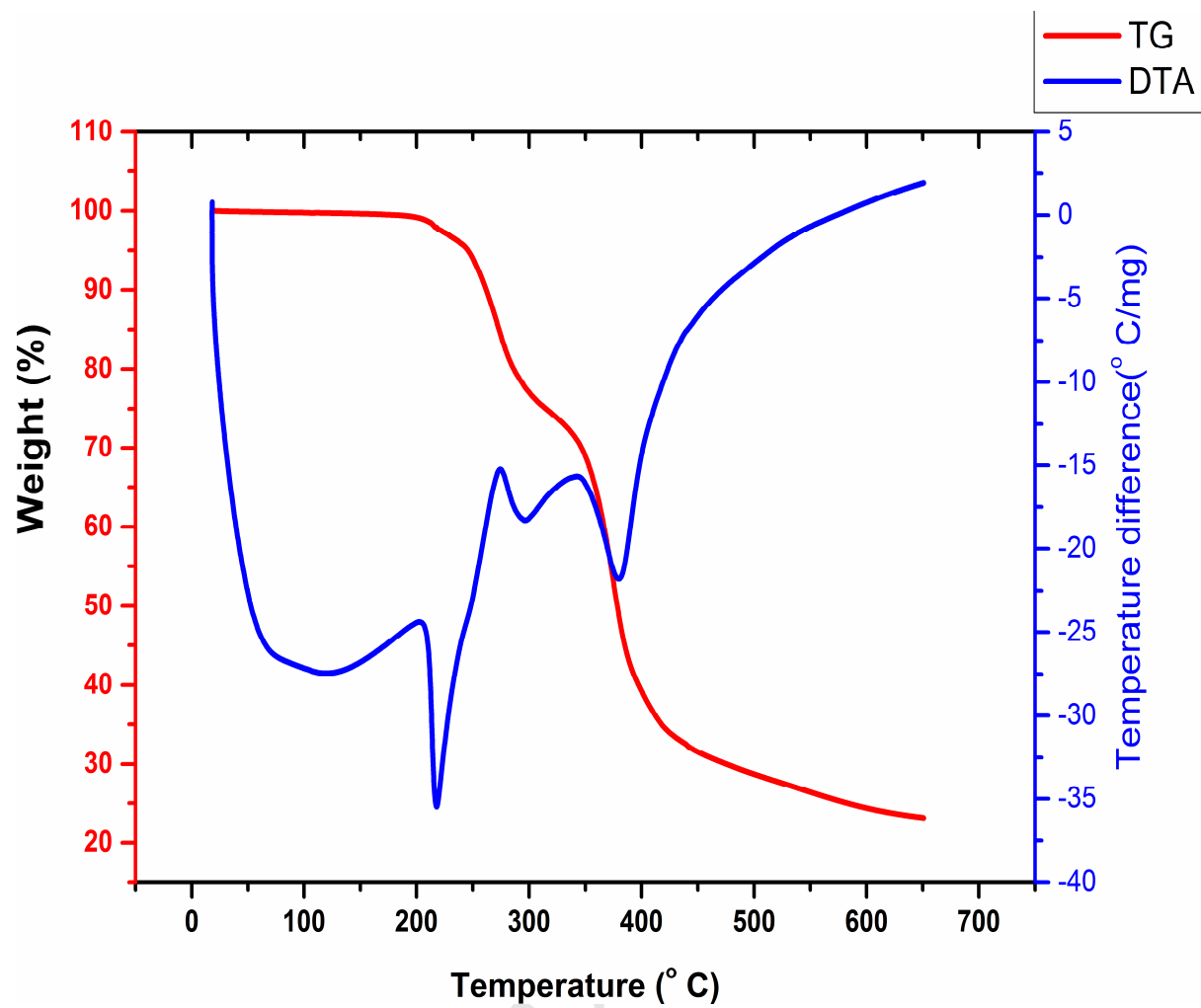


Fig. 11. TGA/DTA plot of 4MPMAB crystal

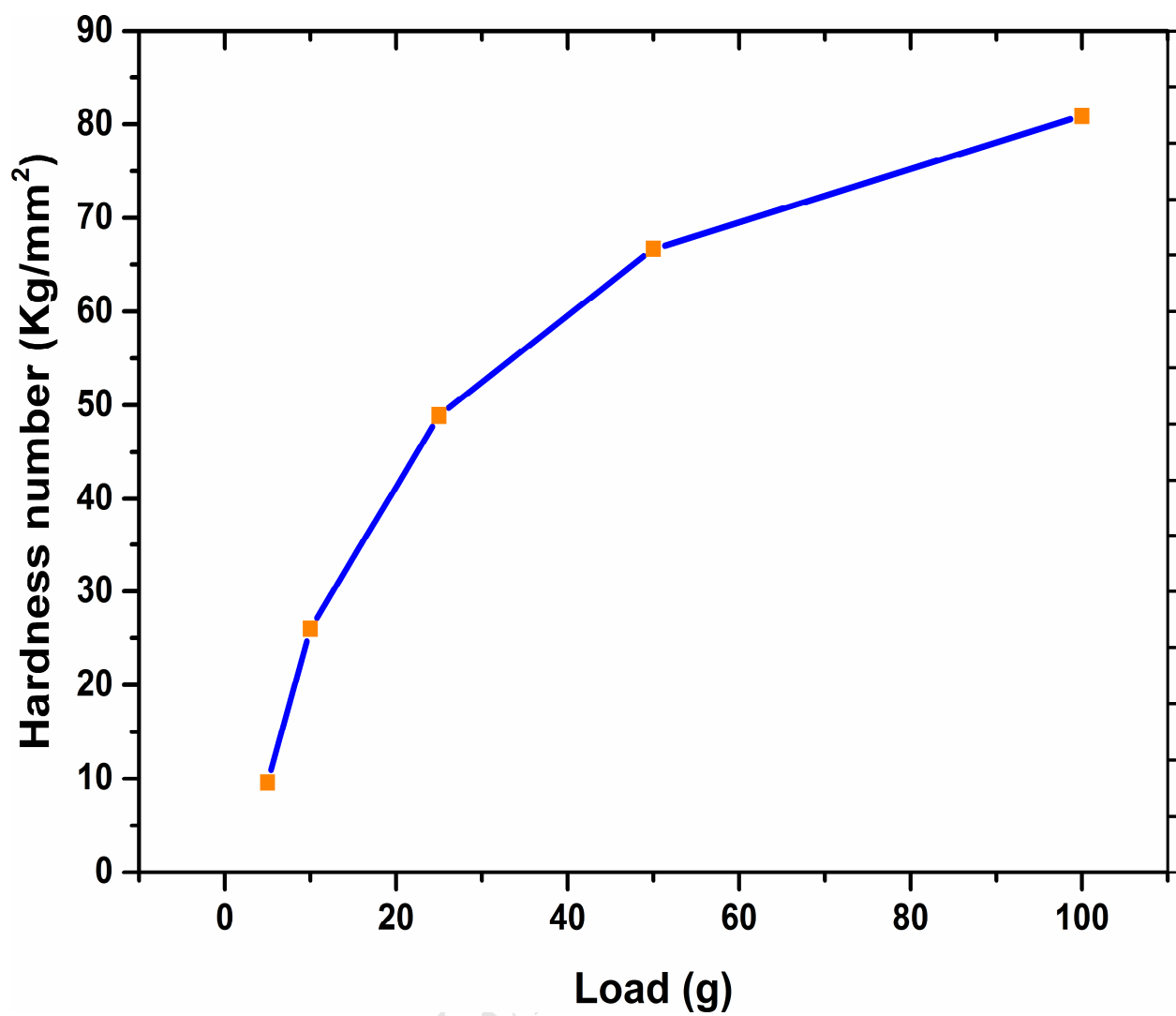


Fig. 12. Variation of hardness number on applied indentation load of 4MPMAB crystal

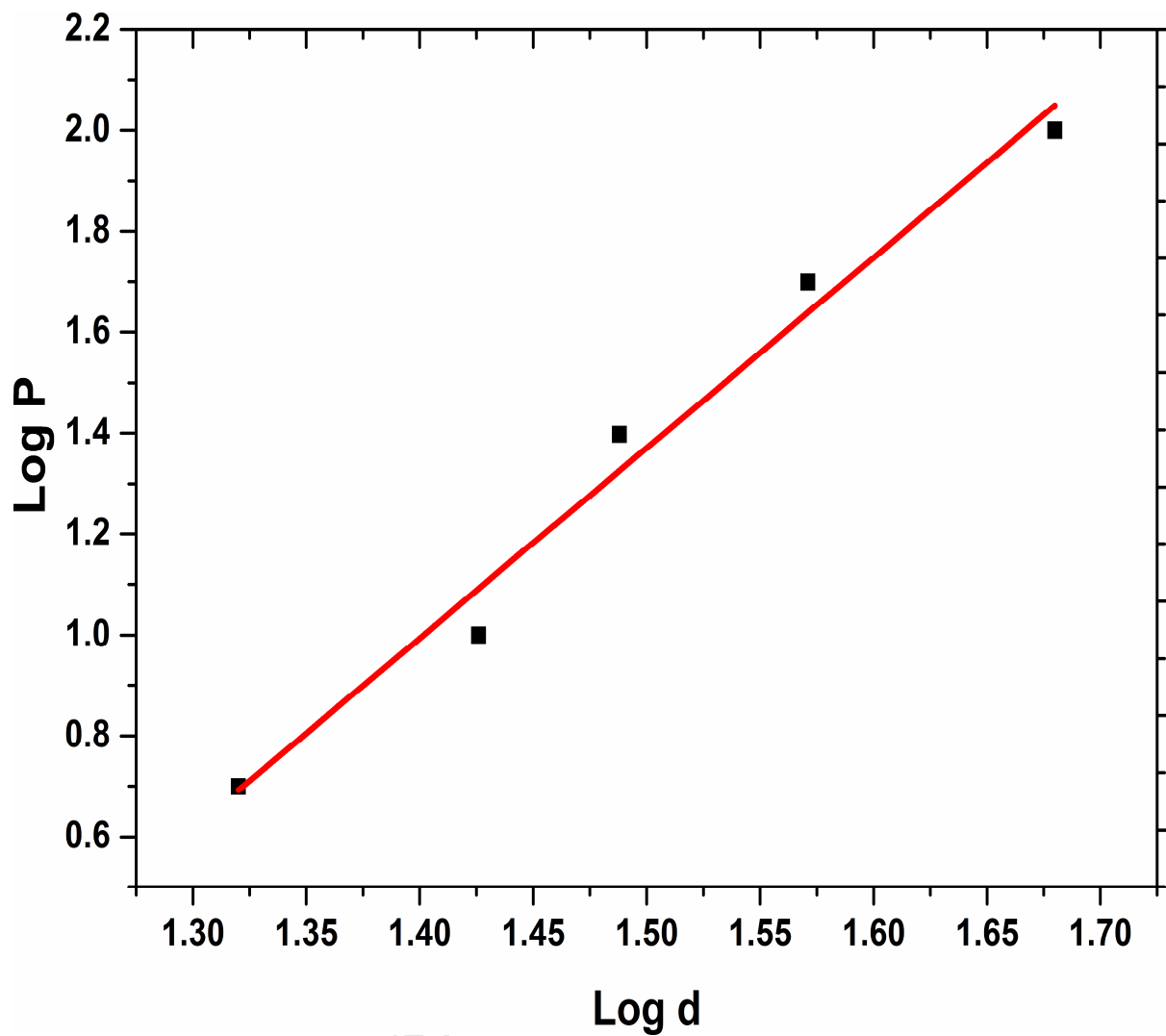


Fig. 13. The plot of log P vs log d of 4MPMAB crystal

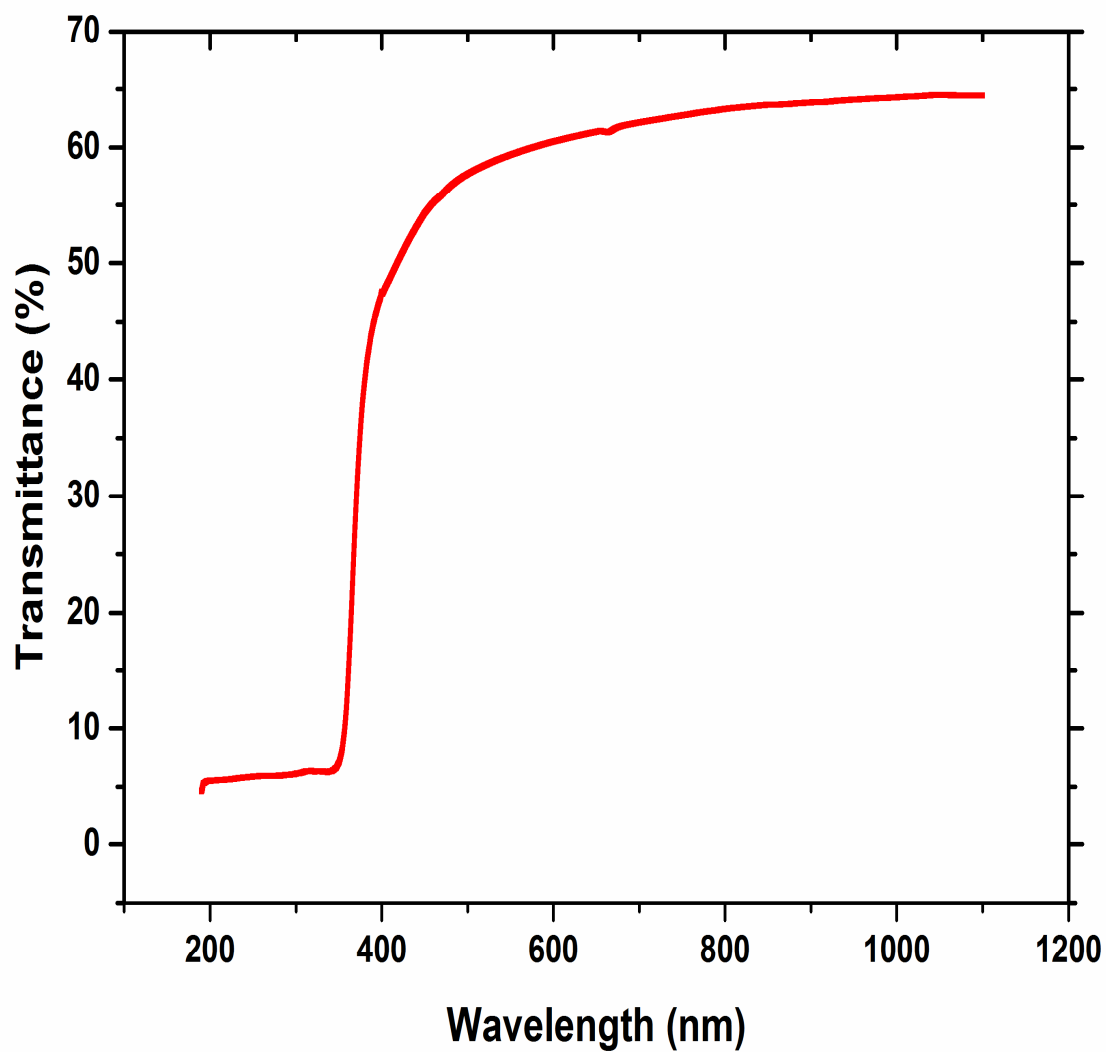


Fig. 14. Transmission spectrum of 4MPMAB crystal

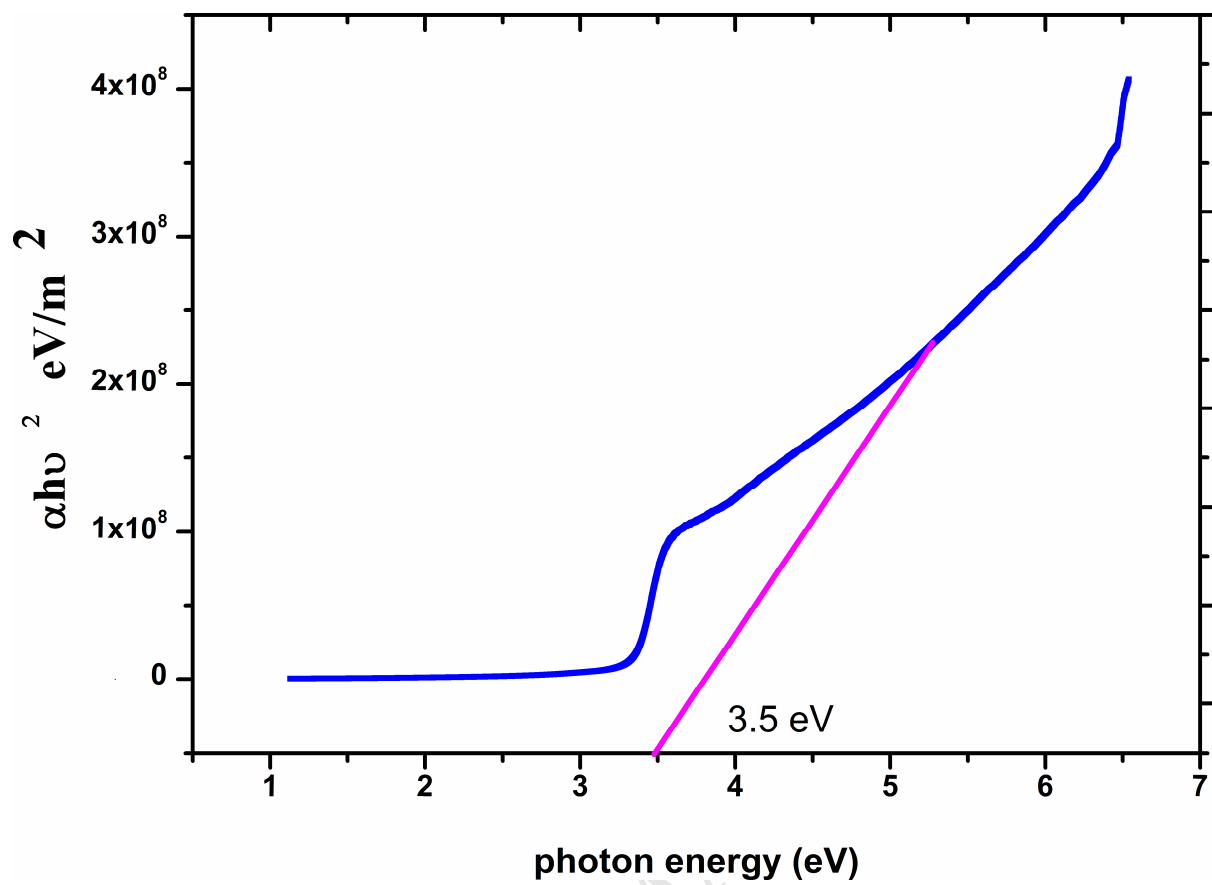


Fig. 15. Tauc's plot of 4MPMAB crystal

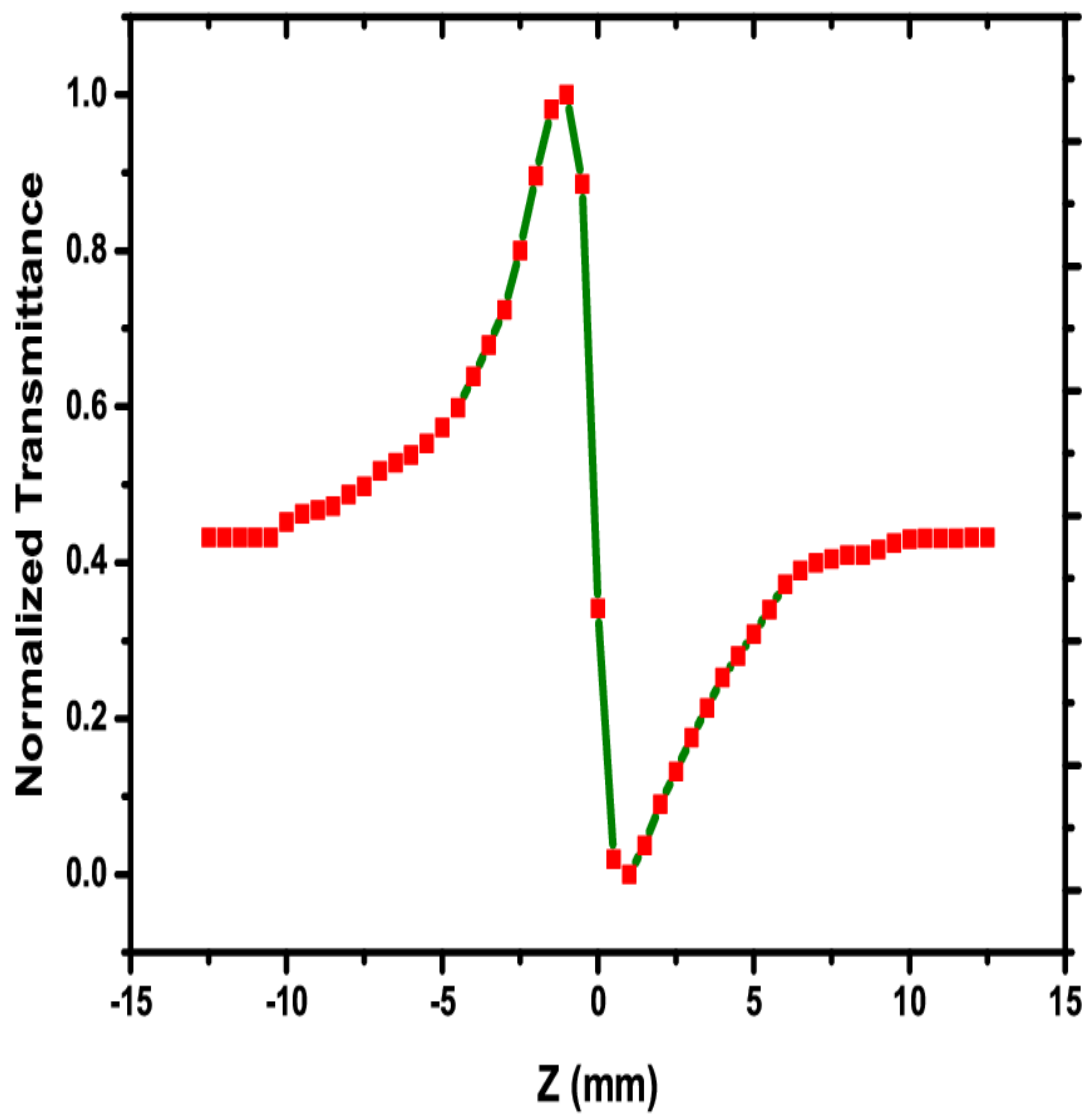


Fig. 16. Closed aperture Z-scan curve of the 4MPMAB crystal

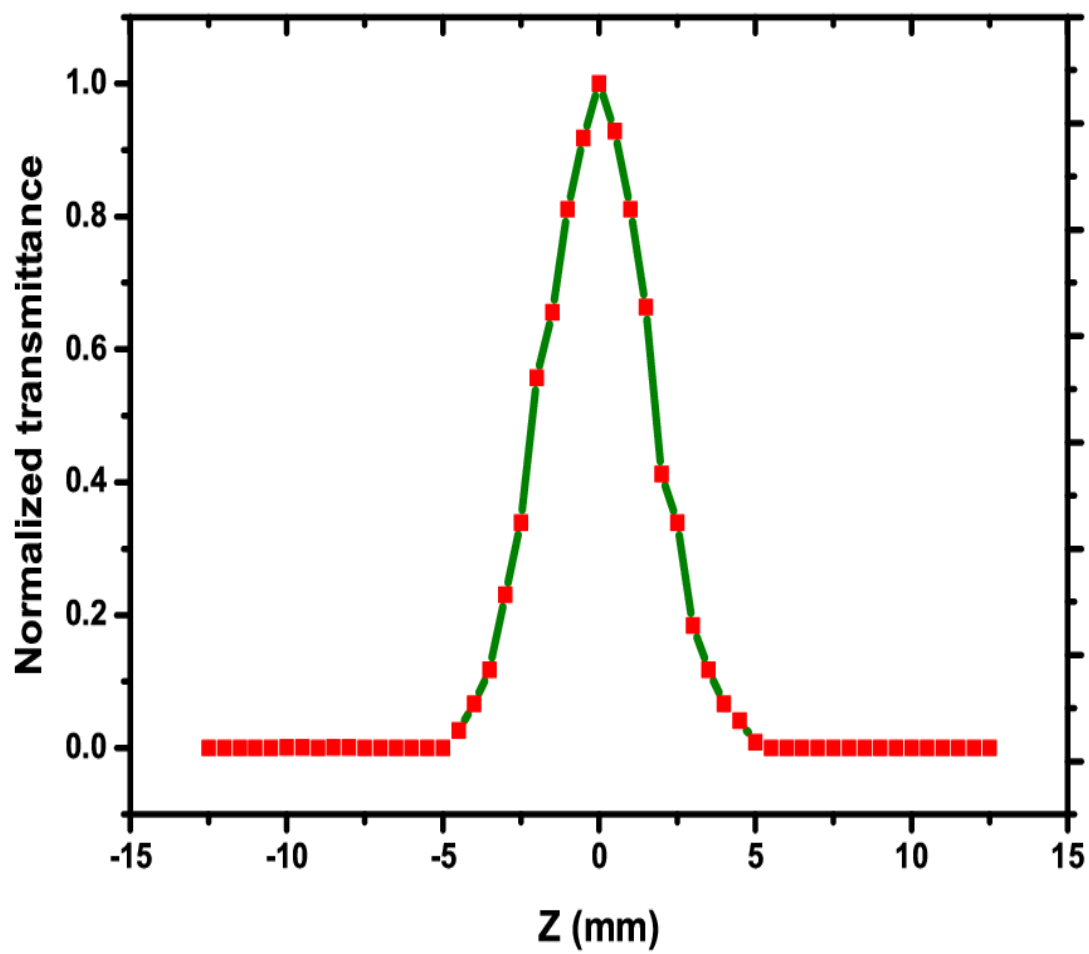


Fig. 17. Open aperture Z-scan curve of the 4MPMAB crystal

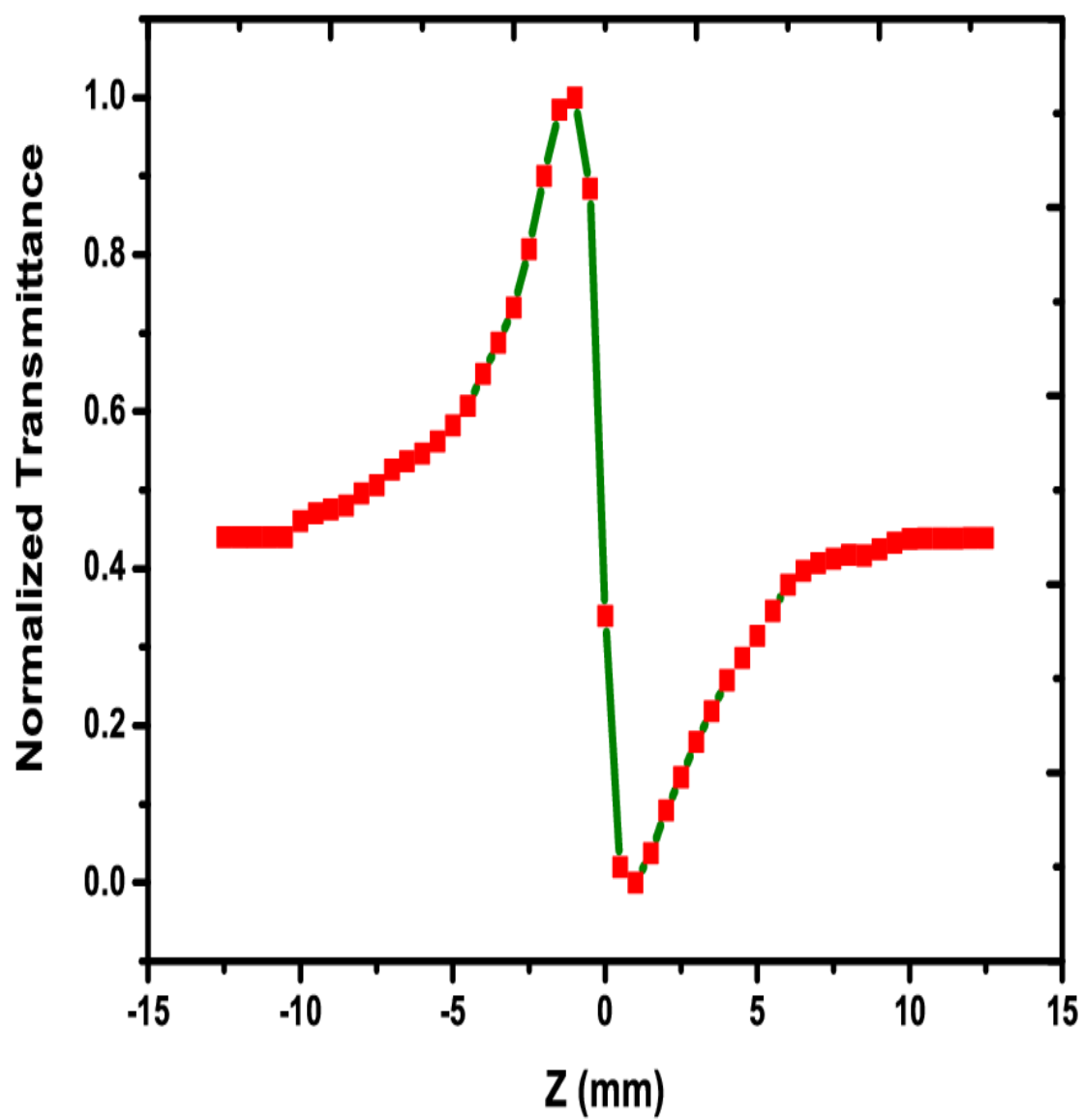


Fig. 18. The ratio of open to closed aperture Z-scan curve of the 4MPMAB crystal

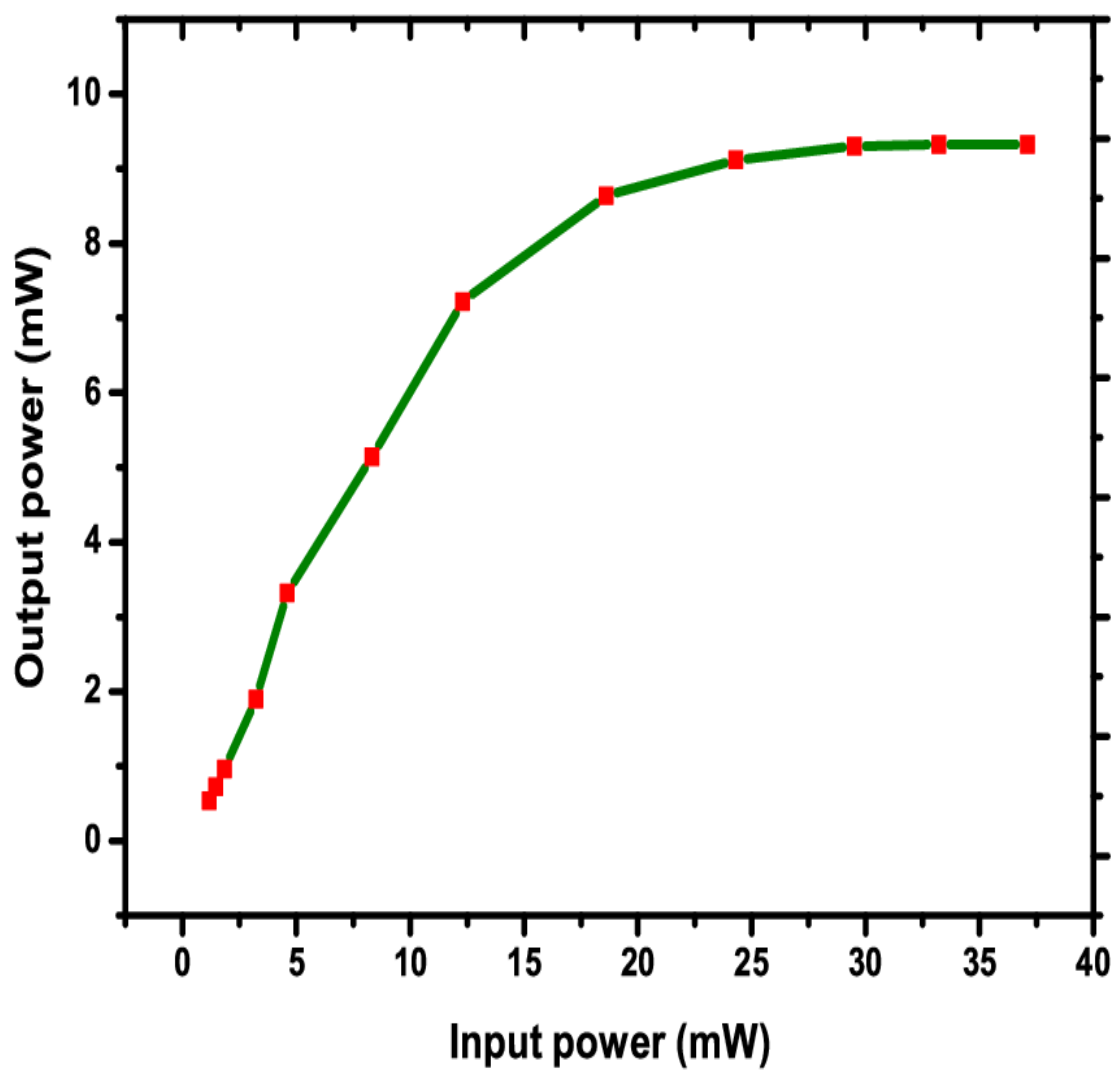
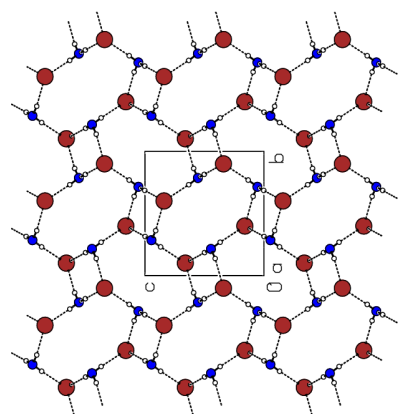


Fig. 19. The optical limiting curve of 4MPMAB crystal

Highlights

- New crystal 4MPMAB belongs to monoclinic crystal system and centrosymmetric spacegroup $P2_1/c$.
- Influence of various hydrogen bonding interaction on spectral, third-order nonlinear optical properties were explored.
- The relationship between structure and third-order NLO properties were revealed.
- 4MPMAB shows wide optical transmission from 330 nm to 1100 nm.
- The crystal exhibits higher third-order nonlinearity and the optical limiting behavior confirms that 4MPMAB crystal is a promising candidate for optical limiting applications.



ACCEPTED MANUSCRIPT